

# The Amyloid Precursor Protein Regulates Synaptic Transmission at Medial Perforant Path Synapses

Maximilian Lenz,<sup>1,2</sup> Amelie Eichler,<sup>1</sup> Pia Kruse,<sup>1</sup> Christos Galanis,<sup>1</sup>  Dimitrios Kleidonas,<sup>1,3,4</sup> Geoffroy Andrieux,<sup>5</sup> Melanie Boerries,<sup>5,6</sup> Peter Jedlicka,<sup>7,8,9</sup> Ulrike Müller,<sup>10</sup> Thomas Deller,<sup>8</sup> and  Andreas Vlachos<sup>1,11,12</sup>

<sup>1</sup>Department of Neuroanatomy, Institute of Anatomy and Cell Biology, Faculty of Medicine, University of Freiburg, 79104 Freiburg, Germany, <sup>2</sup>Hannover Medical School, Institute of Neuroanatomy and Cell Biology, 30625 Hannover, Germany, <sup>3</sup>Spemann Graduate School of Biology and Medicine, University of Freiburg, 79104 Freiburg, Germany, <sup>4</sup>Faculty of Biology, University of Freiburg, 79104 Freiburg, Germany, <sup>5</sup>Institute of Medical Bioinformatics and Systems Medicine, Medical Center, Faculty of Medicine, University of Freiburg, 79104 Freiburg, Germany, <sup>6</sup>German Cancer Consortium, German Cancer Research Center, 69120 Heidelberg, Germany, <sup>7</sup>Interdisciplinary Centre for 3Rs in Animal Research, Faculty of Medicine, Justus-Liebig-University, 35392 Giessen, Germany, <sup>8</sup>Institute of Clinical Neuroanatomy, Neuroscience Center, Goethe University Frankfurt, 60590 Frankfurt am Main, Germany, <sup>9</sup>Frankfurt Institute for Advanced Studies, 60438 Frankfurt am Main, Germany, <sup>10</sup>Institute of Pharmacy and Molecular Biotechnology, Functional Genomics, Ruprecht-Karls University Heidelberg, 69120 Heidelberg, Germany, <sup>11</sup>Center for Basics in Neuromodulation, Faculty of Medicine, University of Freiburg, 79104 Freiburg, Germany, and <sup>12</sup>Center BrainLinks–BrainTools, University of Freiburg, 79104 Freiburg, Germany

The perforant path provides the primary cortical excitatory input to the hippocampus. Because of its important role in information processing and coding, entorhinal projections to the dentate gyrus have been studied in considerable detail. Nevertheless, synaptic transmission between individual connected pairs of entorhinal stellate cells and dentate granule cells remains to be characterized. Here, we have used mouse organotypic entorhino-hippocampal tissue cultures of either sex, in which the entorhinal cortex (EC) to dentate granule cell (GC; EC–GC) projection is present, and EC–GC pairs can be studied using whole-cell patch-clamp recordings. By using cultures of wild-type mice, the properties of EC–GC synapses formed by afferents from the lateral and medial entorhinal cortex were compared, and differences in short-term plasticity were identified. As the perforant path is severely affected in Alzheimer's disease, we used tissue cultures of amyloid precursor protein (APP)–deficient mice to examine the role of APP at this synapse. APP deficiency altered excitatory neurotransmission at medial perforant path synapses, which was accompanied by transcriptomic and ultrastructural changes. Moreover, presynaptic but not postsynaptic APP deletion through the local injection of Cre-expressing adeno-associated viruses in conditional *APP<sup>flox/flox</sup>* tissue cultures increased the neurotransmission efficacy at perforant path synapses. In summary, these data suggest a physiological role for presynaptic APP at medial perforant path synapses that may be adversely affected under altered APP processing conditions.

**Key words:** amyloid precursor protein; dentate gyrus; entorhinal cortex; hilar mossy cell; perforant path; stellate cells

Received Sep. 24, 2022; revised May 20, 2023; accepted May 24, 2023.

Author contributions: M.L. and A.V. designed research; M.L., A.E., P.K., C.G., D.K., P.J., performed research; M.L., A.E., P.K., G.A., M.B., and P.J. analyzed data; and M.L., A.E., P.K., G.A., M.B., P.J., U.M., T.D., and A.V. wrote the paper.

This work was supported by Else Kröner-Fresenius-Stiftung Grant EKFS\_#2019\_A94 to M.L.; Deutsche Forschungsgemeinschaft (DFG) Collaborative Research Centre Transregio (CRC/TRR) Grants 167 Project-ID 259373024-Z01, CRC1160 Project ID 256073931-Z02, CRC1453 Project ID 431984000-S1, and CRC1479 Project ID 441891347-S1 to M.B.; DFG Grant CRC/TRR 167 Project-ID 259373024 B14 to A.V.; DFG Grant Project 467764793 JE 528/10-1 to P.J.; and DFG Grant Forschergruppe (FOR) 1332 ID 138733498 to U.M., T.D., and A.V. The Galaxy server used for some calculations is in part funded by CRC 992 Medical Epigenetics DFG Grant SFB 992/1 201 and German Federal Ministry of Education and Research (BMBF) Grants 031 A538A/A538C RBC, 031L0101B/031L0101C German Network for Bioinformatics Infrastructure (de.NBI)-epi, and 031L0106

Structured Analysis and Integration of RNA-Seq experiments (de.NBI); BMBF Grant MIRACUM-FKZ 01ZZ1801B to M.B.; BMBF Grant EkoEstMed FKZ 01ZZ2015 to G.A.; and BMBF Grant OGEAM-2 16LW0161K to U.M. and T.D. We thank Simone Zenker and Sigrun Nestel for technical assistance, Hanna Hemeling for support with data analysis, and Dr. R. Jude Samulski and the University of North Carolina Vector Core for providing adeno-associated viruses AAV2-hSyn-GFP-Cre.

Thomas Deller has received an honorarium from Novartis for a lecture on human brain anatomy. All the other authors declare no competing financial interests.

Correspondence should be addressed to Maximilian Lenz at lenz.maximilian@mh-hannover.de or Andreas Vlachos at andreas.vlachos@anat.uni-freiburg.de.

<https://doi.org/10.1523/JNEUROSCI.1824-22.2023>

Copyright © 2023 the authors

### Significance Statement

The hippocampus receives input from the entorhinal cortex via the perforant path. These projections to hippocampal dentate granule cells are of utmost importance for learning and memory formation. Although there is detailed knowledge about perforant path projections, the functional synaptic properties at the level of individual connected pairs of neurons are not well understood. In this study, we investigated the role of APP in mediating functional properties and transmission rules in individually connected neurons using paired whole-cell patch-clamp recordings and genetic tools in organotypic tissue cultures. Our results show that presynaptic APP expression limits excitatory neurotransmission via the perforant path, which could be compromised in pathologic conditions such as Alzheimer's disease.

### Introduction

The dentate gyrus is the gateway to the hippocampus (Winson and Abzug, 1977; Hsu, 2007; Krook-Magnuson et al., 2015), receiving input from cortical areas and recurrent fibers from hippocampal regions (Patton and McNaughton, 1995; Amaral et al., 2007; Ribak and Shapiro, 2007). Therefore, signal integration and processing in this region are of considerable interest in understanding dedicated hippocampal features (Leutgeb et al., 2007; Leutgeb and Moser, 2007; Jonas and Lisman, 2014), such as memory formation (Trimper et al., 2017), space and time orientation (GoodSmith et al., 2017), and complex behavior implementation (Senzai and Buzsáki, 2017; Hainmueller and Bartos, 2018).

Dentate granule cells (GCs) are the predominant cell type within the dentate gyrus. They receive their major excitatory inputs from the perforant path and recurrent fibers originating from the hilar region (Amaral et al., 2007). The perforant path originating from layer 2 principal neurons of the entorhinal cortex (EC) forms asymmetric synapses at GC dendrites in the outer two thirds of the molecular layer (Forster et al., 2006). These axons span the entire transverse extent of the molecular layer (Tamamaki and Nojyo, 1993). Multiple studies have identified the distinct features of the projection, such as short-term plasticity (STP) expression, using local electric stimulation and field-potential recordings (Winkels et al., 2009; Jedlicka et al., 2012; Petersen et al., 2013). However, perforant path synapses at the level of individual neuron pairs, that is, layer 2 stellate cells in the EC and dentate GCs, remain to be investigated.

Beyond its role in normal brain function, the perforant path has been recognized as a major component in memory formation and neuropsychiatric diseases (Kirkby and Higgins, 1998; Roy et al., 2016; Smith and McMahan, 2018). Among these diseases, Alzheimer's disease is associated with progressive alterations along the perforant path that correlate with cognitive decline (Robinson et al., 2014). In this context, the processing of the amyloid precursor protein (APP), and specifically synaptotoxic amyloid- $\beta$  (A $\beta$ ), has been associated with the pathogenic plaque formation and cognitive decline in Alzheimer's disease. Moreover, proteolytic amyloidogenic APP cleavage at perforant path terminals was found to regulate synaptic transmission and hippocampal function (Lazarov et al., 2002; Harris et al., 2010; Soldano and Hassan, 2014). Nevertheless, the impact of APP on synaptic transmission at individual perforant path synapses remains unknown.

In this study, we investigated the characteristics of excitatory neurotransmission onto dentate GCs originating from both the hilar mossy cells and the EC at the level of individual neuron pairs. Moreover, we addressed the physiological role of APP in synaptic transmission at the EC-GC synapse. We show the distinct electrophysiological features of excitatory inputs to dentate

GCs using paired whole-cell patch-clamp recordings in organotypic entorhino-hippocampal tissue cultures prepared from wild-type and APP-deficient mice of either sex. Our results demonstrate that presynaptic but not postsynaptic APP deficiency is accompanied by increased excitatory synaptic transmission efficacy between connected neuron pairs at the medial perforant path. Consistent with these findings, an ultrastructural analysis identified a significant increase in the number of docked vesicles at presynaptic active zones in the molecular layer of the APP-deficient dentate gyrus. These results disclose the synaptic properties of the entorhino-hippocampal pathway at the level of individually connected pairs of neurons and demonstrate that presynaptic APP is a key regulator of excitatory synaptic transmission at perforant path synapses in the dentate gyrus.

### Materials and Methods

#### Ethics statement

Mice were maintained in a 12 h light/dark cycle with food and water available *ad libitum*. Every effort was made to minimize distress and pain of animals. All experimental procedures were performed according to the German animal welfare legislation and approved by the animal welfare committee and/or the animal welfare officer at Goethe University Frankfurt, Faculty of Medicine, and University of Freiburg, Faculty of Medicine.

#### Preparation of organotypic tissue cultures

Entorhino-hippocampal tissue cultures were prepared at postnatal day 4–5 from C57BL/6J and APP-deficient ( $APP^{-/-}$ ; null allele; Li et al., 1996; Heber et al., 2000) animals of either sex as previously described (Del Turco and Deller, 2007). Briefly, the dorsal brain surface was immobilized on cutting plates with Histoacryl (B. Braun), and transverse sectioning was performed using a vibratome (VT1200S, Leica). The entorhino-hippocampal complex was dissected from 300  $\mu$ m transverse sections containing the entorhinal cortex and ventral hippocampus (Fig. 1) and placed on porous filter membranes (catalog #PICM0RG50, Millipore). Compared with hippocampus-only tissue cultures, mossy cell axons are limited to the inner molecular layer of the dentate gyrus, and ectopic mossy fiber sprouting cannot be observed (Becker et al., 2012). Conditional APP-deficient cultures were prepared from homozygous  $APP^{lox/lox}$  animals (Mallm et al., 2010) of either sex that were crossed to  $B6.Cg-Gt(ROSA)26Sor^{tm14(CAG-tdTomato)Hze/J}$  ( $Ai14^{+/-}$ ; catalog #007914, The Jackson Laboratory; Madisen et al., 2010). The newly generated mouse line ( $Ai14-APP^{lox/lox}$ ) is a reporter mouse revealing nuclear recombination by cellular tdTomato expression. Here, both the promoter and exon 1 of the APP gene were flanked by loxP sites, which results in cell-type-specific null alleles on Cre-recombination (Mallm et al., 2010). Cultivation medium contained 50% (v/v) MEM, 25% (v/v) basal medium eagle, 25% (v/v) heat-inactivated normal horse serum, 25 mM HEPES buffer solution, 0.15% (w/v) bicarbonate, 0.65% (w/v) glucose, 0.1 mg ml<sup>-1</sup> streptomycin, 100 U ml<sup>-1</sup> penicillin, and 2 mM GlutaMAX. The pH was adjusted to 7.3, and the medium was replaced three times per week. All tissue cultures were allowed to mature for at least 18 d in humidified atmosphere with 5% CO<sub>2</sub> at

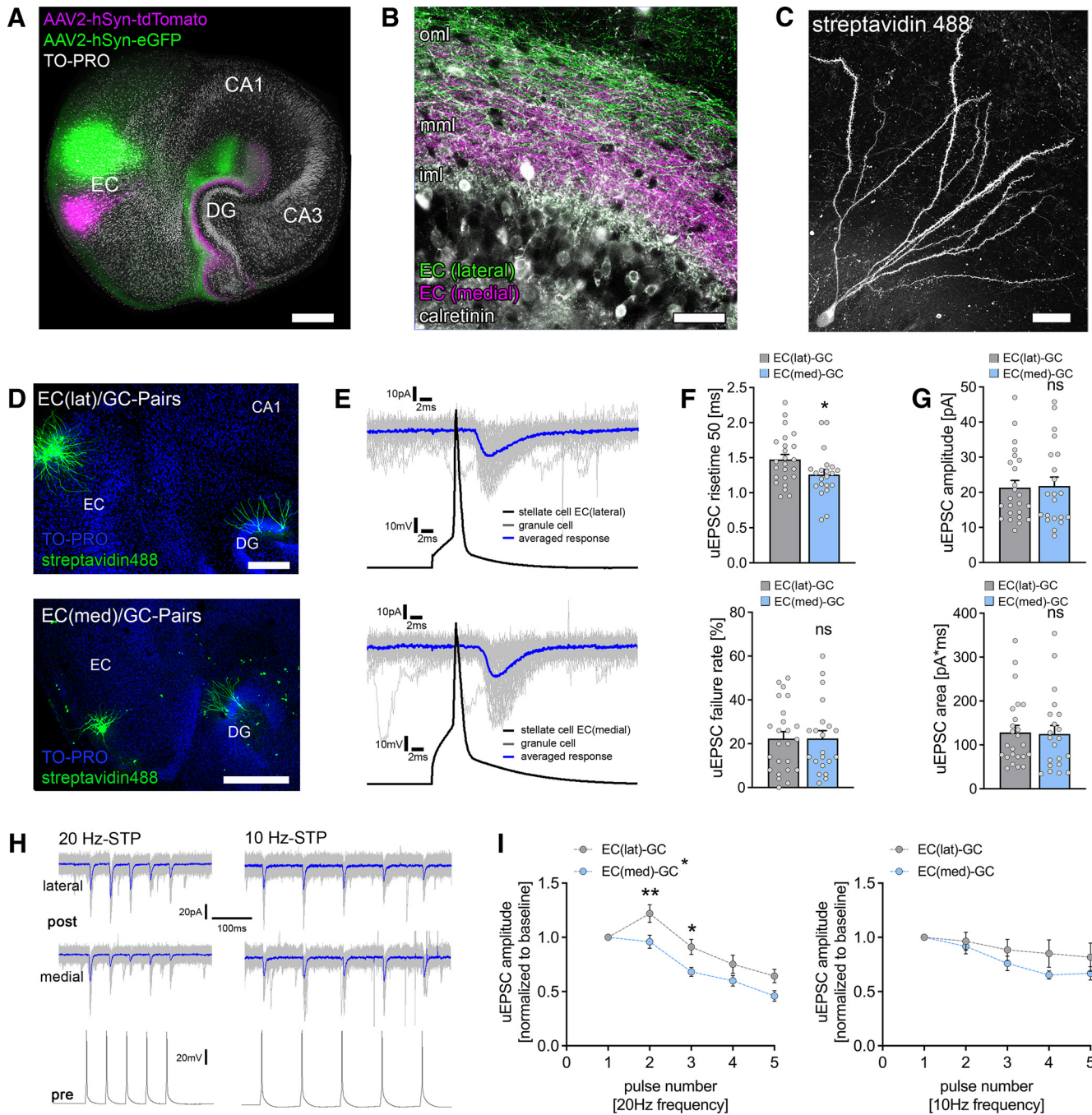


**Figure 1.** Functional characterization of laminar innervation of dentate granule cells in organotypic entorhino-hippocampal tissue cultures. **A**, Overview of a mouse organotypic entorhino-hippocampal tissue culture stained with TO-PRO nuclear stain (white) to visualize cytoarchitecture. The entorhino-hippocampal projection is visualized by a perforant path tracing using AAV-mediated expression of tdTomato (medial part) and eGFP (lateral part) in the entorhinal cortex. Scale bar, 300  $\mu$ m. DG, Dentate gyrus. **B**, The dentate gyrus at higher magnification demonstrating its laminar innervation. eGFP-labeled axonal projections from the lateral part of the entorhinal cortex reach the outer molecular layer (oml), whereas tdTomato-labeled fibers project to the middle molecular layer (mml). The inner molecular layer (iml) that contains hilar mossy cell axons (visualized by calretinin immunostaining) is not innervated by entorhino-hippocampal projections. Scale bar, 50  $\mu$ m. **C**, *Post hoc* streptavidin-stained dentate granule cell. Scale bar, 20  $\mu$ m. **D**, *Post hoc* staining of paired recordings from layer 2 stellate cells in either the lateral (top) or the medial part (bottom) of the entorhinal cortex and dentate granule cells in the suprapyramidal blade of the dentate gyrus. TO-PRO nuclear stain was used to visualize cytoarchitecture. Scale bars: (top) 200  $\mu$ m; (bottom) 300  $\mu$ m. **E**, Action potentials were induced in EC stellate cells (50 action potentials, black trace), and postsynaptic responses were recorded in dentate granule cells (gray traces, single sweeps; blue trace, averaged response). **F**, Synaptic failure rate was not significantly different between paired recordings from the lateral and the medial part of the perforant path. Nevertheless, monosynaptic connections between the medial layer 2 stellate cells and dentate granule cells had significantly faster rise times ( $n_{\text{EC(lat)-GC}} = 24$  pairs in 9 tissue cultures;  $n_{\text{EC(med)-GC}} = 21$  pairs in 10 tissue cultures; Mann–Whitney test,  $U = 162$ ). **G**, No differences in uEPSC amplitude or area were found between connected neuronal pairs of the lateral and the medial perforant path (Mann–Whitney test). **H**, Sample traces for STP experiments at either 20 or 10 Hz presynaptic action potential induction. Blue traces indicate averaged responses. **I**, Short-term plasticity was assessed by the induction of five action potentials at 20 and 10 Hz frequency in presynaptic stellate cells (20 Hz,  $n_{\text{EC(lat)-GC}} = 24$  pairs in 9 tissue cultures;  $n_{\text{EC(med)-GC}} = 21$  pairs in 10 tissue cultures; 10 Hz,  $n_{\text{EC(lat)-GC}} = 11$  pairs in 4 tissue cultures;  $n_{\text{EC(med)-GC}} = 9$  pairs in 4 tissue cultures; normalized to first response/baseline). EC(lat)-GC pairs displayed a synaptic facilitation at 20 Hz, whereas neither facilitation nor depression was seen at 10 Hz presynaptic stimulation. In contrast, EC(med)-GC showed in both 20 Hz and 10 Hz presynaptic stimulation neither synaptic facilitation nor depression in response to the second presynaptic action potential. lat, Lateral; med, medial. Repetitive stimulation of both pathways resulted in progressive synaptic depletion, which seemed more prominent in 20 Hz stimulation. Thus, significant differences between the individual pathways on repetitive presynaptic stimulation at the synaptic level were identified (RM 2-way ANOVA with Sidak’s multiple comparisons test). Individual data points are indicated by gray dots. Values represent mean  $\pm$  SEM (\* $p < 0.05$ , \*\* $p < 0.01$ ; ns, not significant).

35°C because at this age a steady state in structural and functional properties of the organotypic tissue cultures is reached (Hailer et al., 1996; Vlachos et al., 2012b, 2013b; Humpel, 2015). Experiments were conducted in dentate granule cells from the suprapyramidal blade. Because of the three-dimensional orientation of the hippocampus, the cultured dentate gyrus may show morphologic variations of the infrapyramidal blade in some tissue cultures.

#### Perforant path tracing and local viral Cre-GFP expression

Adeno-associated viruses (AAVs) obtained from SignaGen Laboratories (both  $10^{13}$  vg/ml, 1:4 diluted in PBS; AAV2-Synapsin-tdTOMATO, catalog #SL100896; AAV2-Synapsin-GFP, catalog #SL100817) and the University of North Carolina Vector Core ( $10^{12}$  vg/ml, 1:4 diluted in PBS; catalog #AAV2-hSyn-GFP-Cre) were injected into the entorhinal cortex at 3–5 d *in vitro* with a Zeiss Axioscope 2 equipped with a 4× objective (air, NA 0.1) using borosilicate glass pipettes (cf. Lenz et al., 2019). Cultures were returned to the incubator immediately after injection and allowed to mature for at least 18 d in a humidified atmosphere with 5% CO<sub>2</sub> at 35°C.

#### Immunohistochemistry

Cultures were fixed in a solution of 4% (w/v) paraformaldehyde (PFA) in PBS (0.1 M, pH 7.4) and 4% (w/v) sucrose for 1 h. Fixed cultures were incubated for 1 h with 10% (v/v) normal goat serum (NGS) in 0.5% (v/v) Triton X-100-containing PBS to block nonspecific staining. To label calcretinin, whole-tissue cultures were incubated with rabbit anti calcretinin (1:1000; catalog #214102, Synaptic Systems) in PBS containing 10% (v/v) NGS and 0.1% (v/v) Triton X-100 at 4°C overnight. Cultures were washed and incubated for 3 h with appropriate secondary antibodies (1:1000 in PBS with 10% normal goat serum (NGS) or normal horse serum (NHS), 0.1% Triton X-100; Invitrogen). TO-PRO or DAPI (1:5000 in PBS for 10 min; TO-PRO, catalog #T-3605, Invitrogen; DAPI, catalog #62248, Thermo Fisher Scientific) nuclear stain was used to visualize cytoarchitecture. Sections were washed, transferred onto glass slides, and mounted for visualization with anti-fading mounting medium (Dako Fluoromount).

Confocal images in immunostainings were acquired using a Leica SP8 confocal microscope equipped with a 60× objective lens (NA 1.4).

#### Post hoc staining

Cultures were fixed in a solution of 4% (w/v) PFA in PBS (0.1 M), pH 7.4, and 4% (w/v) sucrose for 1 h. Fixed cultures were incubated for 1 h with 10% (v/v) NGS in 0.5% (v/v) Triton X-100-containing PBS. Biocytin filled cells were counterstained with Alexa Fluor 488 or Alexa Fluor 647 conjugated streptavidin (1:1000 in PBS with 10% NGS, 0.1% Triton X-100; catalog #S-32354 and catalog #S-32357, Invitrogen, respectively) for 4 h and DAPI or TO-PRO staining was used to visualize cytoarchitecture (1:5000 in PBS for 10 min; TO-PRO, catalog #T-3605, Invitrogen; DAPI, catalog #6248, Thermo Fisher Scientific). Slices were washed, transferred, and mounted onto glass slides for visualization with anti-fading mounting medium (Dako Fluoromount). Confocal images were acquired using a Nikon Eclipse C1si laser-scanning microscope with a 4× objective lens (NA 0.2, Nikon), a 20× objective lens (NA 0.9, Nikon) and a 60× objective lens (NA 1.4, Nikon) or a Leica SP8 confocal microscope equipped with a 40× objective lens (NA 1.3). Detector gain and amplifier were initially set to obtain pixel intensities within a linear range.

#### Transmission electron microscopy

*APP*<sup>+/+</sup> and *APP*<sup>-/-</sup> tissue cultures were fixed in 4% paraformaldehyde (w/v) and 2% glutaraldehyde (w/v) in 0.1 M phosphate buffer (PB) overnight and washed for 1 h in 0.1 M PB. After fixation, tissue cultures were sliced with a vibratome, and the slices were incubated with 1% osmium tetroxide for 20 min in 5% (w/v) sucrose containing 0.1 M PB. The slices were washed 5 times for 10 min in 0.1 M PB and washed in graded ethanol [10 min in 10% (v/v) and 10 min in 20 (v/v)]. The slices were then incubated with uranyl acetate [1% (w/v) in 70% (v/v) ethanol] overnight and subsequently dehydrated in graded ethanol, 80% (v/v), 90% (v/v), and 98% (v/v) for 10 min. Finally, slices were incubated with 100% (v/v) ethanol two times for 15 min followed by two 15 min washes with propylene oxide. The slices were then transferred for 30 min in a 1:1 mixture of propylene oxide with Durcupan and then for 1 h in Durcupan. The

Durcupan was exchanged for fresh Durcupan, and the slices were stored at 4°C overnight. The slices were then embedded between liquid release-coated slides and coverslips. Cultures were re-embedded in blocks, and ultrathin sections were collected on copper grids. Electron microscopy was performed with a LEO 906E microscope (Zeiss) at 4646× magnification. Acquired images were saved as TIF files and analyzed using ImageSP Viewer software (<http://e.informer.com/sys-prog.com>). In each group, 50 synapses from 5 independent tissue cultures were analyzed in the distal parts of the molecular layer. Asymmetric spine synapses were identified, and the total amount of presynaptic vesicles and docked vesicles to presynaptic active zones were manually quantified by an investigator blind to the genotype.

#### Paired whole-cell patch-clamp recordings

Whole-cell voltage-clamp recordings from dentate granule cells of slice cultures were conducted at 35°C (two–five neurons per culture). The bath solution contained the following (in mM): 126 NaCl, 2.5 KCl, 26 NaHCO<sub>3</sub>, 1.25 NaH<sub>2</sub>PO<sub>4</sub>, 2 CaCl<sub>2</sub>, 2 MgCl<sub>2</sub>, and 10 glucose. For EPSC recordings, patch pipettes contained the following (in mM): 126 K-glucuronate, 4 KCl, 4 Mg-ATP, 0.3 Na<sub>2</sub>-GTP, 10 phosphocreatine, 10 HEPES, and 0.3% (w/v) biocytin, pH, 7.25 (with KOH, 290 mOsm with sucrose), having a tip resistance of 4–6 MΩ. In some experiments Alexa Fluor 488 was added to the internal solution to visualize neuronal morphology before recordings. Cells were visually identified using an LN-Scope (Luigs & Neumann) or a Zeiss LSM750 equipped with infrared dot contrast and a 40× water-immersion objective (NA, 0.8; Olympus). Granule cells were patched in the outer third of the granule cell layer. Electrophysiological signals were amplified using a MultiClamp 700B amplifier, digitized with a Digidata 1550B digitizer, and visualized with the pCLAMP 11 software package. Neurons were recorded at a holding potential of –70 mV. To avoid recording immature granule cells, recordings were discarded if the initial resting membrane potential was higher than –70 mV. Hilar mossy cells were identified during the experiment by their morphologic and electrophysiological features (Scharfman and Schwartzkroin, 1988; Henze and Buzsaki, 2007), that is, large multipolar cell body, sag-current on hyperpolarization, small or absent after-hyperpolarization on action potential induction, resting membrane potential higher than –70 mV, and synaptic connection (depolarizing) to postsynaptic dentate granule cell. Recordings were discarded if series resistance reached ≥30 MΩ. Action potentials were generated in the presynaptic cell by 5 ms square current pulses (1 nA) elicited at 0.2 Hz (up to 50 pulses) while recording unitary EPSCs (uEPSCs) from dentate granule cells. Neurons were considered to be connected if >5% of action potentials evoked time-locked inward uEPSCs. For short-term plasticity, five action potentials were applied at 10 or 20 Hz, respectively (intersweep-interval, 5 s, up to 30 repetitions).

#### Regional mRNA library preparation and transcriptome analysis

RNA library preparations for transcriptome analysis were performed using the NEBNext Single Cell/Low Input RNA Library Prep Kit for Illumina (catalog #E6420, New England Biolabs) according to manufacturer instructions. Briefly, isolation of the dentate gyrus from individual tissue cultures was performed using a scalpel. One isolated dentate gyrus was transferred to 7.5 μl lysis buffer (supplemented with murine RNase inhibitor) and homogenized using a pestle. Samples were centrifuged for 30 s at 10000 × g, and 5 μl of supernatant were collected from individual samples and further processed. After cDNA synthesis, cDNA amplification was performed according to the protocol of the manufacturer with 12 PCR cycles. The cDNA yield was subsequently analyzed by a High Sensitivity DNA assay on a Bioanalyzer instrument (Agilent). The amount of cDNA was adjusted to 10 ng for further downstream applications. After fragmentation and adaptor ligation, dual index primers (catalog #E7600S, New England Biolabs) were ligated in a library amplification step using 10 PCR cycles. Libraries were finally cleaned with 0.8× Solid Phase Reversible Immobilization beads (catalog #B23318, Beckman Coulter) following a standard bead purification protocol. Library purity and size distribution were assessed

with a High Sensitivity DNA assay on a Bioanalyzer instrument (Agilent). We quantified the libraries using the NEBNext Library Quant Kit for Illumina (catalog #E7630, New England Biolabs) based on the mean insert size provided by the Bioanalyzer. A 10 nM sequencing pool (120  $\mu$ l in Tris-HCl, pH 8.5) was generated for sequencing on the NovaSeq 6000 sequencing platform (Illumina; service provided by CeGaT). We performed a paired-end sequencing with 150 bp read length. Data analysis was performed on the Galaxy Europe platform (<https://usegalaxy.eu/>; Galaxy Community, 2022). All files contained >10 million high-quality reads (after mapping to reference genome; mm10) with a Phred quality of at least 30 (>90% of total reads).

#### Compartmental modeling

Compartmental simulations of synaptic EPSCs in dentate granule cells were performed as described previously (Vlachos et al., 2012a) using the simulation environment T2N (Trees-to-NEURON interface; Beining et al., 2017) linking MATLAB (version 2018b, MathWorks) and NEURON (version 7.4; Hines and Carnevale, 1997; [www.neuron.yale.edu](http://www.neuron.yale.edu)) software. Briefly, we used eight reconstructed morphologies of mouse dentate granule cells (Schmidt-Hieber et al., 2007) from the ModelDB system (accession #95960). Passive biophysical properties were adjusted to match the intrinsic properties of wild-type granule cells in organotypic tissue cultures from Galanis et al. (2021). Excitatory (AMPA-like) synaptic currents were simulated using a double-exponential conductance change with a peak amplitude of 0.06 nS, a rise time of 0.2 ms, a decay time of 2.5 ms, and a reversal potential of 0 mV. To determine the dependence of simulated EPSC amplitudes on the distance from the soma, identical single synaptic input was activated at different locations along a path between the soma and a distal end of the dendrite, and corresponding EPSCs were detected at the soma. Simulated cells were voltage clamped at  $-70$  mV. To simulate compound EPSCs, we monitored voltage clamped somatic currents in eight model granule cells in which synaptic activity was triggered by sequential activation of a single dendritic AMPA synapse placed at decreasing distances in one dendritic branch or by synchronous activation of dendritic AMPA synapses placed at equidistant locations in all dendritic branches.

#### Experimental design and statistical analysis

**Study design.** In this study, we used age-matched organotypic entorhino-hippocampal tissue cultures in a prospective study design. Each tissue culture represents a biological replicate that defines independent experiments. Excitatory inputs onto dentate granule cells were analyzed in age-matched tissue cultures in which one pathway was tested per tissue culture with one to five postsynaptic cells. Only one tissue culture per mouse was used for the investigation of a distinct pathway. Each pair is considered a biological replicate. To elucidate the role of APP in synaptic transmission, age-matched APP-deficient and C57BL/6J cultures were compared (see Figs. 4, 5). In the localized APP-recombination experiments (see Fig. 6), tissue cultures from  $APP^{fllox/fllox} \times Ai14$  Cre reporter mice were used, and recombination was achieved by local viral injection of AAV-hSyn-Cre-GFP. For postsynaptic recombination, viral injections were performed in the dentate gyrus. For presynaptic recombination, viral injections were performed in the medial part of the entorhinal cortex. Recombination was determined during the patch-clamp experiments by visual inspection of the tdTomato signal.

**Quantification.** Electrophysiological data were analyzed using pCLAMP 10.7 (Molecular Devices) and MiniAnalysis (Synaptosoft) software. The fraction of action potentials not followed by time-locked EPSC responses was considered as synaptic failure rate. The uEPSC amplitude, rise time (rise50), and area were assessed in uEPSCs from successfully transmitted action potentials, as well as the mean amplitude of all successfully evoked postsynaptic responses. For evaluation of short-term plasticity experiments, recorded traces were averaged in Clampfit 10.7 software, regardless of successful synaptic transmission at individual pulses. In some analyses, postsynaptic responses were normalized to the first response in averaged traces.

Presynaptic ultrastructural features were analyzed in randomly selected perforant path terminals from electron micrographs of the outer parts of the molecular layer. Postsynaptic features of the same set of images were analyzed in a previous study (Galanis et al., 2021). Presynaptic terminals and vesicles were manually assessed by an investigator blind to experimental conditions.

RNA sequencing data were uploaded to the Galaxy web platform (public server, <https://usegalaxy.eu/>; Afgan et al., 2016, 2018; Jalili et al., 2020) and transcriptome analysis was performed using the Galaxy platform in accordance with the reference-based RNA-seq data analysis tutorial (Batut et al., 2021). Adapter sequences, low quality, and short reads were removed via the cutadapt tool (Galaxy version 3.5+galaxy0). Reads were mapped using the RNA STAR tool (Galaxy version 2.7.8a+galaxy0) with the mm10 full reference genome (Mus musculus). The evidence-based annotation of the mouse genome (GRCm38), version M25 (Ensembl 100), served as gene model (GENCODE). For an initial assessment of gene expression, unstranded featureCount (Galaxy version 2.0.1+galaxy2) analysis was performed from RNA STAR output. Only samples that contained >60% uniquely mapping reads (feature, exon) were considered for further analysis. Genes with a low number of mean reads (<50 counts) were excluded from further analysis. Read counts were further processed with R software (version 4.2.1). Differential gene expression analysis was performed with DESeq2 R package (version 1.36; Love et al., 2014) using the Wald significance test. Gene-set enrichment analysis was performed with the clusterProfiler package in R (version 4.4.4; Wu et al., 2021) using gene sets from the Molecular Signatures Database (MSigDB; version 7.2; Subramanian et al., 2005). In both analyses, the adjusted *p* value below 0.05 was set as significant threshold.

**Statistical analysis.** Data were statistically analyzed using GraphPad Prism 9 software. For statistical comparison of two experimental groups, a Mann–Whitney test was used. For the evaluation of datasets with three experimental groups, a Kruskal–Wallis test followed by Dunn's *post hoc* correction was performed. Short-term plasticity experiments were statistically assessed by the repeated measure (RM) two-way ANOVA test with Sidak's multiple comparisons test. uEPSC amplitude values from individual cells were stacked in subcolumns, and pulse number defined tabular rows (COLUMN factor, pathway, genetic background or recombination; ROW factor, pulse number); *p* values <0.05 were considered statistically significant (\**p* < 0.05, \*\**p* < 0.01, \*\*\**p* < 0.001). The numbers (*n*) are provided in the figure legends. Results that did not yield significant differences were designated not significant (ns). Statistical differences in *x*, *y* plots are indicated by an asterisk in the figure legends when detected through multiple comparisons. In the text and figures, values represent the mean  $\pm$  SEM unless otherwise indicated.

#### Digital illustrations

Confocal image stacks were stored as TIF files. Figures were prepared using the ImageJ software package (<https://imagej.nih.gov/ij/>) and Photoshop graphics software (Adobe). Image brightness and contrast were adjusted.

#### Data availability

Source data with statistical evaluations are provided on the Dryad data repository (<https://doi.org/10.5061/dryad.tdz08kq2x>). Raw data (fastq-files) used for transcriptome analysis are available at the Gene Expression Omnibus (accession number GSE213284). The code for compartmental modeling is available via the Zenodo repository. (<https://doi.org/10.5281/zenodo.7503491>) Original data are available from the corresponding authors on reasonable request.

## Results

### Laminar innervation of the dentate gyrus in organotypic entorhino-hippocampal tissue cultures

The perforant path was visualized in the dentate gyrus of organotypic entorhino-hippocampal tissue cultures using local viral injections of AAV vectors expressing either green fluorescent protein (GFP) or tandem dimer Tomato (tdTomato) under the

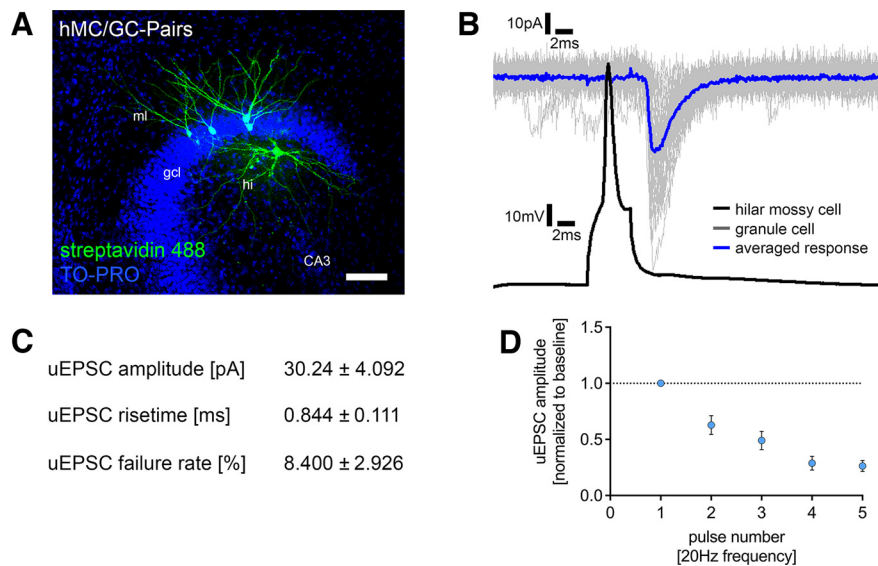


**Figure 2.** Single-cell characterization of the hilar mossy cell–dentate granule cell projection. **A**, *Post hoc* staining of paired recordings from hilar mossy cells (hMC) and dentate granule cells in the suprapyramidal blade of the dentate gyrus. TO-PRO nuclear stain was used to visualize cytoarchitecture. Scale bar, 100  $\mu$ m. gcl, granule cell layer; ml, molecular layer; hi, hilar region. **B**, Action potentials were induced in hilar mossy cells (50 action potentials, black trace), and postsynaptic responses were recorded in dentate granule cells (gray traces, single sweeps; blue trace, averaged response). Connected pairs showed highly reliable inward currents on presynaptic stimulation. **C**, Summary table for single-cell characterization of excitatory inputs onto dentate granule cells, originating from hilar mossy cells (5 pairs in 21 tissue cultures). **D**, Short-term plasticity experiments revealed a depressive and depletive behavior of this connection following repetitive stimulation. Values represent mean  $\pm$  SEM.

control of a synapsin promoter. Injections were performed in the medial (tdTomato-expression) and lateral parts (GFP-expression) of the entorhinal cortex in the same set of cultures (Fig. 1A). Indeed, GFP-positive axons originating from neurons in the lateral part of the cultured entorhinal cortex were readily detected in the outer molecular layer (oml) of the dentate gyrus. In contrast, tdTomato-labeled axons in the same cultures were observed in the middle molecular layer (mml; Fig. 1B). In addition, mossy cell axons were observed in the inner molecular layer (iml) using calretinin immunostainings in AAV-traced tissue cultures (Fig. 1B), confirming the organotypic, that is, *in vivo*-like, laminar innervation of the dentate gyrus (Frotscher and Heimrich, 1995; Forster et al., 2006).

### Paired whole-cell patch-clamp recordings show lamina-specific differences in the STP of perforant path synapses

The entorhino-hippocampal projections were characterized at the level of individually connected neuron pairs by simultaneously patching layer 2 stellate cells in the lateral or the medial parts of the entorhinal cortex and granule cells in the suprapyramidal blade of the dentate gyrus (Fig. 1C,D). Solitary action potentials were induced in the presynaptic stellate cell while recording excitatory postsynaptic responses from the soma of individual GCs (Fig. 1E). Neurons were considered connected if at least 5% of the presynaptic action potentials induced time-locked uEPSCs in the dentate GC (cf. Vlachos et al., 2012c). Neurons in the lateral and the medial parts of the entorhinal cortex formed direct synaptic connections with dentate GC dendrites. Our analysis showed that the uEPSC rise time was significantly lower in the recorded pairs of medial stellate cells and dentate GCs compared with lateral stellate cells (Fig. 1F; Mann–Whitney test;  $p = 0.04$ ,  $U = 162$ ). Consistent with previous studies that reported a positive correlation between rise time and the synaptic distance from the soma (Sjöström and

Häusser, 2006; Vlachos et al., 2012a; Lenz et al., 2019), this functional result supported our structural analysis showing lamination of excitatory inputs onto dentate GCs (compare Fig. 1A,B).

The synaptic failure rate, reflecting the number of presynaptic action potentials that failed to elicit postsynaptic responses, did not differ between the medial and the lateral perforant path synapses (Fig. 1F; Mann–Whitney test;  $p = 0.98$ ,  $U = 251$ ). Moreover, the uEPSC amplitude and the area did not differ significantly between the two pathways (Fig. 1G; Mann–Whitney test; uEPSC amplitude,  $p = 0.96$ ,  $U = 249$ ; uEPSC area,  $p = 0.64$ ,  $U = 231$ ), suggesting that medial and lateral perforant path synapses affect somatic membrane potentials equally.

However, an STP assessment inducing five consecutive action potentials (at 20 Hz) in the presynaptic cells showed that the lateral perforant path expressed robust short-term facilitation, which was not seen in the medial perforant path synapses (Fig. 1H; 20 Hz frequency, RM two-way ANOVA with Sidak’s multiple comparisons; pathway,  $p = 0.001$ ,  $F = 6.52$ ; pulse number,  $p < 0.001$ ,  $F = 58.3$ ).

Both pathways showed a synaptic depletion on the fifth pulse. Notably, a 10 Hz presynaptic stimulation did not promote short-term facilitation of the lateral perforant path (Fig. 1H; 10 Hz frequency, RM two-way ANOVA with Sidak’s multiple comparisons; pathway,  $p = 0.31$ ,  $F = 1.09$ ; pulse number,  $p < 0.001$ ,  $F = 9.25$ ). However, the dynamic properties of the medial perforant path projection onto dentate GCs appeared to be independent of presynaptic stimulation frequency. Moreover, synaptic depletion was not as prominent on 10 Hz stimulation. Therefore, subsequent STP experiments were performed at 10 Hz presynaptic stimulation to avoid synaptic depletion. We conclude that the ability to express this frequency-dependent STP form distinguishes perforant path synapses in the oml and mml of the dentate gyrus (Fig. 1H).

### Hilar mossy cell axons in the inner molecular layer form highly reliable synapses onto dentate granule cells

The properties of synapses close to the soma of GCs were assessed using paired recordings between hilar mossy cells and dentate GCs (Fig. 2A). Monosynaptically connected pairs between hilar mossy cells and GCs showed high uEPSC amplitudes, rapid rise times, and low synaptic failure rates (Fig. 2B, C). STP experiments showed a strong depression and fast depletion behavior for mossy cell to GC synapses (Fig. 2D). Notably, previous studies have reported high failure rates of hilar mossy cell projections onto dentate GCs (Scharfman, 1995) and no short-term depression (Hashimoto-dani et al., 2017). This difference may reside in different experimental designs and network effects of extracellular stimulation compensating for synaptic depression at the single-cell level. Regardless of these considerations, we conclude that STP switches from facilitation on distal dendrites to depression on proximal GC dendrites in our experiments.

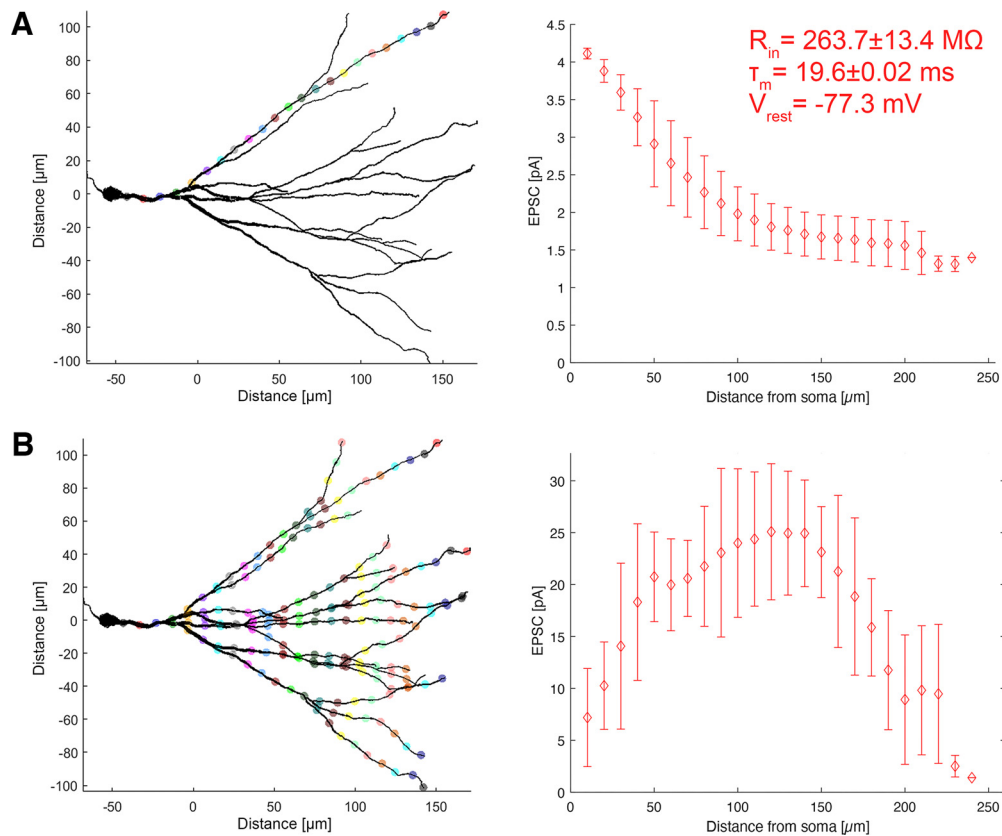


**Figure 3.** Computational modeling of somatic currents elicited by synaptic activation on dentate granule cell dendrites. **A**, Modeling of somatic currents elicited by a single synaptic activation along a specific granule cell dendrite ( $n = 8$  granule cells). Colored dots indicate the location of individual synaptic activation. Right, The *in silico* recorded somatic EPSC depending on the synaptic distance from the granule cell soma with passive properties from organotypic tissue cultures. **B**, Modeling of somatic currents elicited by the simultaneous activation of synapses at granule cell dendrites at distinct distances from the soma. Simultaneously activated synapses are depicted in the same colors. Right, The *in silico* recorded somatic EPSC depending on the synaptic distance from the granule cell soma. Values represent mean  $\pm$  SD.

### Computational modeling of excitatory synaptic inputs indicates a comparable depolarizing impact of the medial and lateral perforant path on dentate granule cells

Previous work showed that dentate GC dendrites strongly attenuate synaptic signals (Krueppel et al., 2011). However, we did not observe differences in uEPSC amplitudes originating from synapses in the oml and mml (compare, Fig. 1G). This finding was further explored by computing the dependence of EPSC amplitude on distance from the soma using compartmental modeling of mouse dentate GCs.

The distribution of simulated EPSCs with increasing distance from the GC layer was determined using identical single synaptic inputs activated at different locations along a path between the soma and a distal end of the dendrite. Corresponding EPSC responses were detected at the soma and the simulated cells were voltage clamped at  $-70$  mV (Fig. 3A). We found a gradual reduction in somatically recorded EPSCs along the dendritic path. This dendritic attenuation stabilized between a 100 and 200  $\mu$ m distance from the soma, which corresponds to the outer two thirds of the molecular layer, that is, mml and oml. Therefore, perforant path synapses of comparable synaptic strength in the mml and oml are expected to depolarize the soma of GCs equally.

Moreover, somatic EPSCs were simulated for the simultaneous activation of excitatory synapses with equal distances from the soma on all GC dendrites. A plateau in somatic EPSC responses was observed, correlating with the layer-specific dendritic complexity (Fig. 3B). Again, these data

suggest that the magnitude of somatic EPSC responses from dendritic synaptic activation remains stable over medium to long distances from the soma.

### Transcriptomic changes in the APP-deficient dentate gyrus

Several factors affecting synaptic transmission at perforant path synapses have been identified, such as alterations in gene expression, epilepsy, or neurodegenerative diseases (Scimemi et al., 2006; Robinson et al., 2014; Jiang et al., 2020). APP and its cleavage products have been recognized as synaptic transmission and plasticity regulators (Müller et al., 2017; Richter et al., 2018; Steubler et al., 2021). Beyond its role in pathologic processes, recent studies suggest a physiological role for APP and its fragments (Zhou et al., 2022). To further characterize the effects of APP deficiency in the dentate gyrus of entorhino-hippocampal tissue cultures, we performed a region-specific transcriptome analysis of dentate gyrus samples isolated from wild-type and APP-deficient tissue cultures (Fig. 4A–F). APP deficiency was associated with complex changes in the gene expression profile within the dentate gyrus (Fig. 4A), where numerous differentially expressed genes were detected (up, 812 genes; down, 1012 genes; unchanged, 12,161 genes; Extended Data Table 4-1; DeSEQ2 package). A gene set enrichment analysis for cellular compartment gene ontologies revealed that the differentially expressed genes could be attributed to distinct gene sets (Fig. 4B,C). Notably, gene sets for differential gene expression were found for ribosomes and synapse-related genes (Fig. 4B,C). A targeted analysis of synapse-related terms identified an

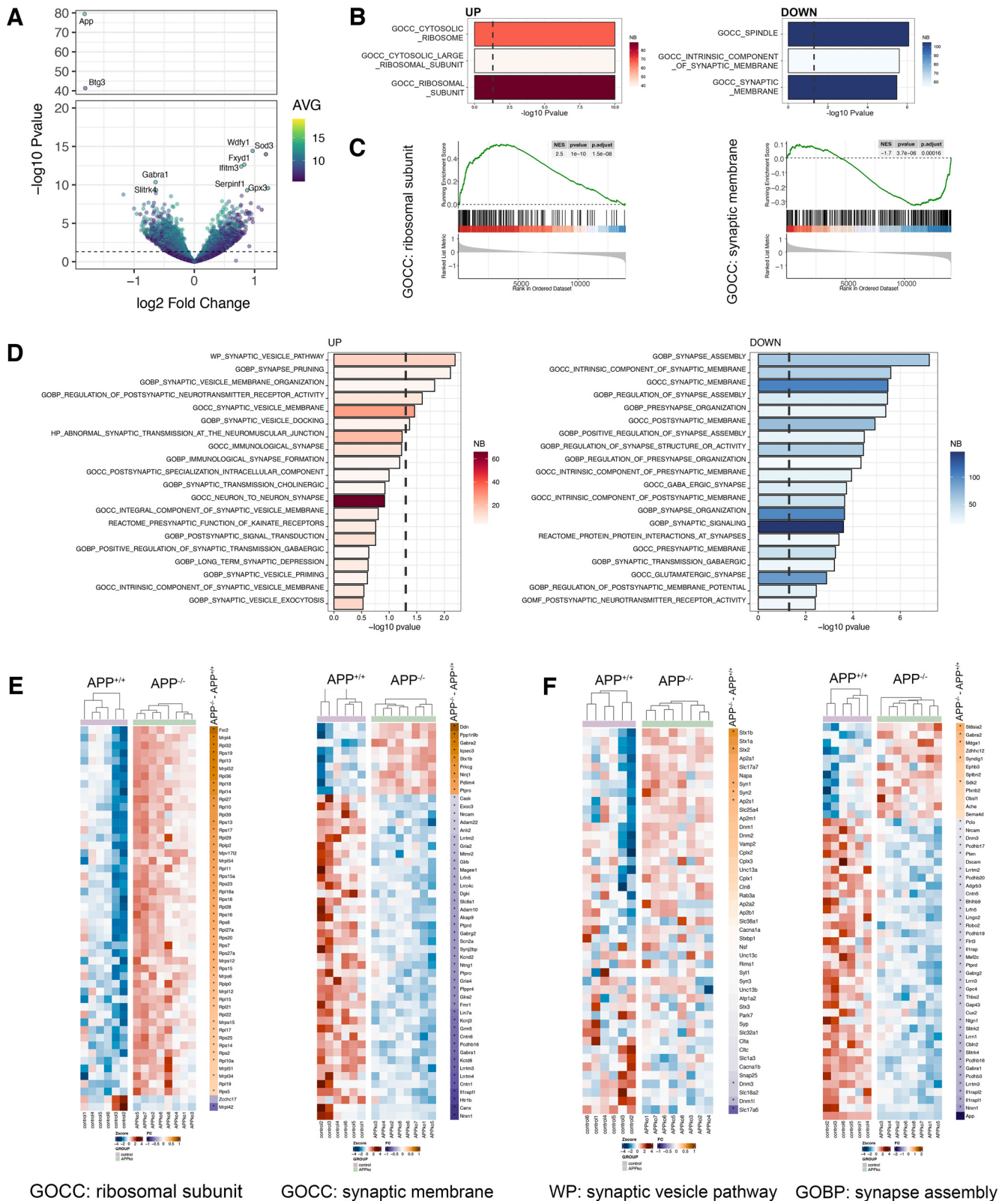


**Figure 4.** APP deficiency modulates the dentate gyrus transcriptome. **A**, Volcano plot showing regulated genes between APP-deficient ( $APP^{-/-}$ ) versus wild type ( $APP^{+/+}$ ;  $n_{APP^{+/+}} = 6$  tissue cultures,  $n_{APP^{-/-}} = 8$  tissue cultures; Extended Data Table 4-1 shows complete differential gene expression analysis). Dashed line indicates the significance threshold [ $-\log_{10}(0.05)$ ]. Right, Color code represents the average (AVG) expression level across all samples. Top ten regulated genes are labeled. **B**, Top three GOCC regulated terms in APP-deficient versus wild type. Right, Color codes represent the number (NB) of genes within the gene sets. **C**, Enrichment plot of ribosomal subunit (left) and synaptic membrane (right). Black dashes indicate the ranked list of genes that belong to the respective gene set. **D**, Top twenty upregulated and downregulated terms related to the synapse across the whole MSigDB. Right, Color code represents the number (NB) of genes within the gene sets. **E, F**, Gene level heat maps of selected gene sets from unbiased (**E**, compare **B, C**) and synapse-focused analysis (**F**, compare **D**) showing the row-wise scaled expression (Z-score, left) and the  $\log_2$  fold change between APP-deficient and wild-type cultures (right). The asterisks indicate significant regulation. Genes are ranked according to the  $\log_2$  fold change from high to low.

upregulation of synaptic vesicle-related gene sets [e.g., WikiPathways (WP), synaptic vesicle pathway; Gene Ontology Biological Process (GOBP), synaptic vesicle membrane organization; Gene Ontology Cellular Component (GOCC), synaptic vesicle membrane; GOBP, synaptic vesicle docking] and a downregulation of numerous gene sets related to the presynaptic and postsynaptic organization with their corresponding genes (Fig. 4D,F). Notably, 34 genes related to synaptic vesicle cycle (GOBP, synaptic vesicle cycle) were differentially expressed in APP-deficient tissue cultures, which might hint toward presynaptic phenotypes in synaptic transmission. Thus, APP deficiency leads to complex changes in neural gene expression in the dentate gyrus that might contribute to alterations in excitatory synaptic transmission and plasticity.

### APP deficiency increases excitatory synaptic transmission at medial perforant path synapses

Because of the APP-related differential gene expression in synaptic gene sets, we explored whether APP deficiency affects synaptic transmission between monosynaptically connected medial layer 2 stellate cells and mature dentate GCs (Fig. 5A). APP deficiency was accompanied by a decrease in uEPSC failure rate, indicating increased synaptic reliability (Fig. 5B; Mann–Whitney test;  $p = 0.01$ ,  $U = 25.5$ ). Moreover, the uEPSC amplitude and area were significantly increased in the absence of APP (Fig. 5C; Mann–Whitney test; uEPSC amplitude,  $p = 0.007$ ,  $U = 23$ ; uEPSC area,  $p = 0.003$ ,  $U = 19$ ). The STP experiments confirmed increased uEPSC amplitudes with similar STP dynamics of medial perforant path synapses in the APP-deficient dentate gyrus compared with wild type (Fig. 5D; RM two-way ANOVA with Sidak's multiple comparisons; genotype,  $p = 0.002$ ,  $F = 12.6$ ; pulse number,  $p < 0.001$ ,  $F = 18.8$ ). We conclude that APP regulates the reliability and strength of medial perforant path synapses.

### APP deficiency is accompanied by ultrastructural changes of presynaptic sites at perforant path synapses

To determine whether functional and transcriptomic changes with APP deficiency were accompanied by structural changes in presynaptic and postsynaptic compartments, individual synapses in the molecular layer were examined by transmission electron microscopy (Fig. 5E,F). Notably, in a previous study we did not observe significant postsynaptic changes in APP-deficient tissue cultures (Galani et al., 2021). The analysis of presynaptic features showed that the presynaptic vesicle density was unaltered between the groups (Fig. 5G; Mann–

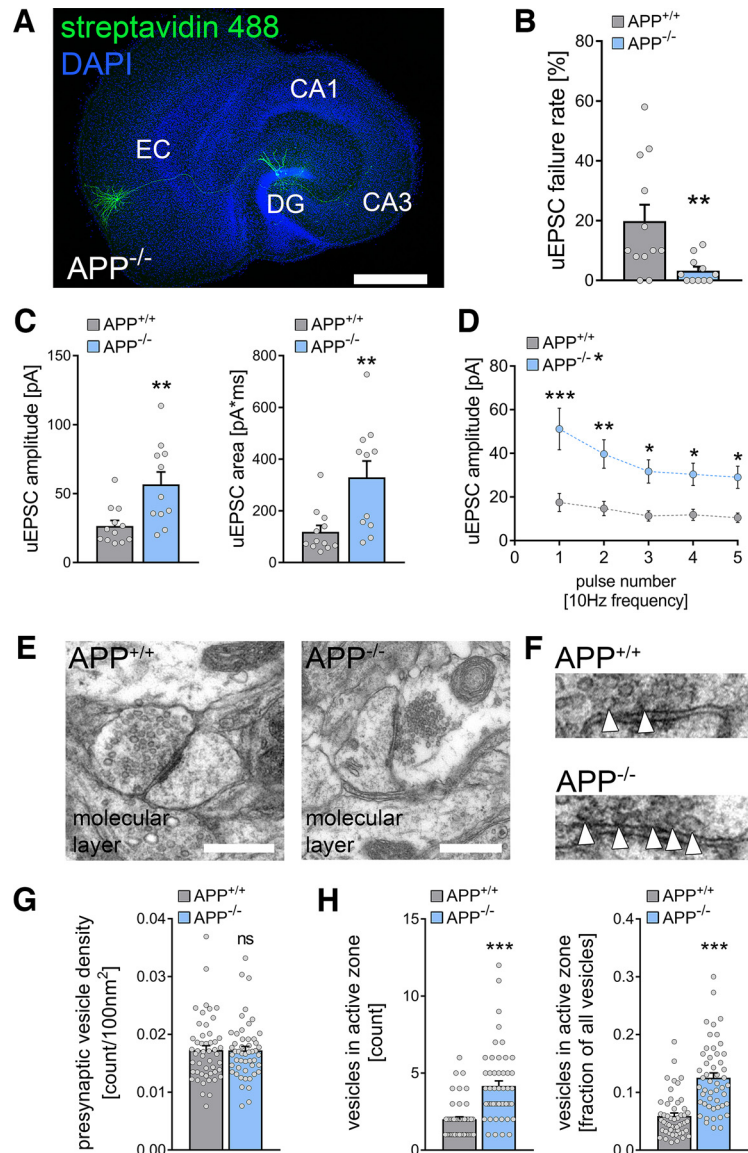


**Figure 5.** Deficiency of the APP increases excitatory synaptic transmission at medial perforant path synapses. **A**, *Post hoc* staining of paired recordings from layer 2 stellate cells in the medial part of the entorhinal cortex and dentate granule cells in the suprapyramidal blade of the dentate gyrus in APP-deficient ( $APP^{-/-}$ ) cultures. DAPI nuclear stain was used to visualize cytoarchitecture. Cultures from APP-deficient animals have no overt morphologic aberration of the perforant path. Scale bar, 500  $\mu$ m. DG, dentate gyrus. **B**, The uEPSC failure rate was significantly reduced in  $APP^{-/-}$  cultures compared with wild-type ( $APP^{+/+}$ ) cultures ( $n_{wildtype} = 12$  pairs in 5 tissue cultures,  $n_{APP-deficient} = 11$  pairs in 5 tissue cultures; Mann–Whitney test,  $U = 25.5$ ). **C**, Both uEPSC amplitude and area were significantly increased in  $APP^{-/-}$  cultures (Mann–Whitney test,  $U_{uEPSC\ amplitude} = 23$ ,  $U_{uEPSC\ area} = 19$ ). **D**, Assessment of short-term plasticity by the application of five presynaptic action potentials at 10 Hz frequency confirmed the increase in uEPSC amplitude with synaptic depletion on repetitive stimulation in  $APP^{-/-}$  cultures (RM 2-way ANOVA with Sidak's multiple comparisons test). **E**, Ultrastructural features of presynaptic perforant path terminals were assessed in electron micrographs of the molecular layer in wild-type ( $APP^{+/+}$ ) and APP-deficient ( $APP^{-/-}$ ) cultures. Scale bars, 500 nm. **F**, Synaptic vesicles were counted in presynaptic boutons. Moreover, the number of vesicles attached to the presynaptic active zone was assessed (white arrowheads). **G**, No difference in presynaptic vesicle density between  $APP^{+/+}$  and  $APP^{-/-}$  preparations was detected ( $n = 50$  presynaptic terminals in each group in three tissue cultures; Mann–Whitney test). **H**, Both the total number of docked vesicles in the presynaptic active zone and the fraction of docked vesicles from the total number of vesicles were increased in APP-deficient tissue preparations (Mann–Whitney test,  $U_{count} = 442.5$ ,  $U_{fraction} = 386$ ). Individual data points are indicated by gray dots. Values represent mean  $\pm$  SEM (\* $p < 0.05$ , \*\* $p < 0.01$ , \*\*\* $p < 0.001$ ; ns, not significant).

Whitney test;  $p = 0.899$ ,  $U = 1231$ ). In contrast, the number and the fraction of vesicles in the presynaptic active zone were significantly increased in APP-deficient tissue cultures [Fig. 5H; Mann–Whitney test; vesicles in active zone (count),  $p < 0.001$ ,  $U = 442.5$ ; vesicles in active zone (fraction),  $p < 0.001$ ,

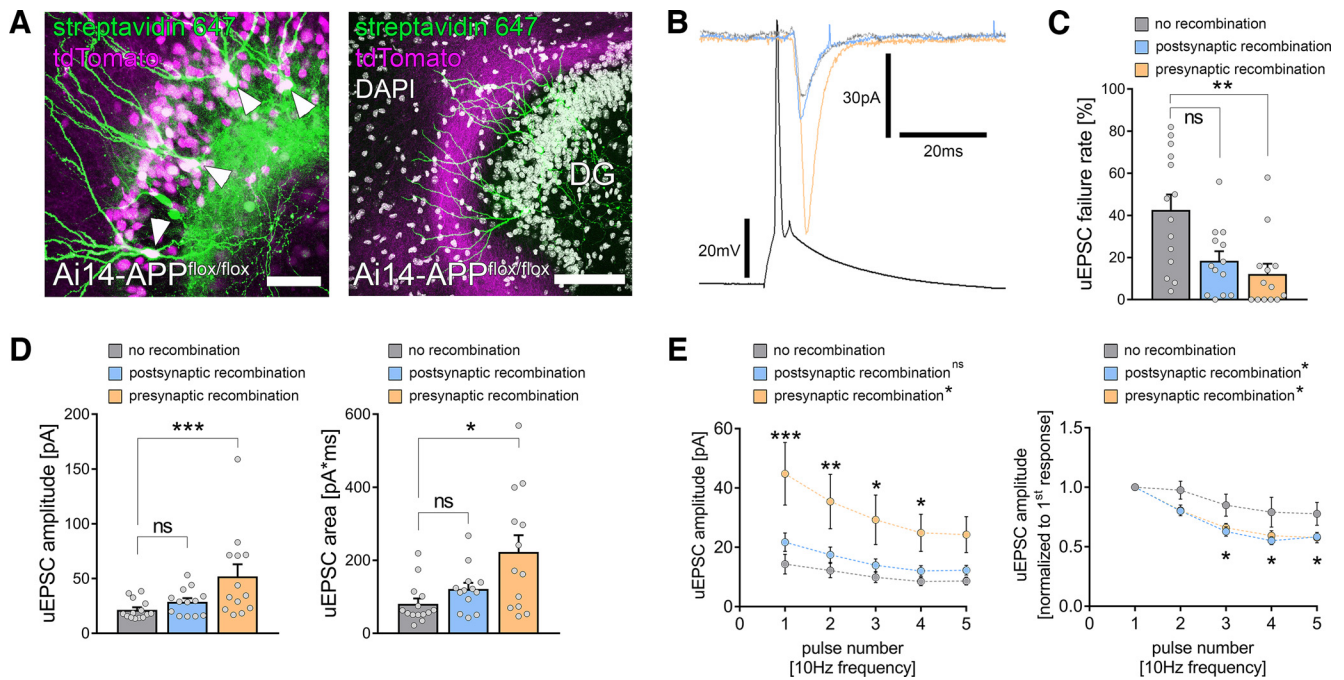


**Figure 6.** Presynaptic APP restrains excitatory neurotransmission at medial perforant path synapses. **A**, To achieve compartment-specific deletion of APP, tissue cultures from *Ai14-APP<sup>flox/flox</sup>* animals were prepared, and region-specific recombination was achieved by a local injection of a Cre-expressing virus in either the dentate gyrus (left) or the medial part of the entorhinal cortex (right). Granule cells (arrowheads, *post hoc* staining with streptavidin 647 of cells that were filled with biocytin during the recording) were patched, and recombination was evaluated during the patch-clamp experiment by the tdTomato signal. Scale bars, (left) 50  $\mu\text{m}$ ; (right) 100  $\mu\text{m}$ . **B**, Electrophysiological properties were assessed in monosynaptic connected pairs of neurons with no recombination (gray trace) or postsynaptic (blue trace) or presynaptic (orange trace) recombination. **C**, The uEPSC failure rate was significantly decreased in connected pairs with presynaptic APP deficiency, whereas postsynaptic APP deficiency resulted in a nonsignificant trend toward increased synaptic reliability ( $n_{\text{no recombination}} = 14$  pairs in 5 tissue cultures;  $n_{\text{postsynaptic recombination}} = 13$  pairs in 5 tissue cultures;  $n_{\text{presynaptic recombination}} = 13$  pairs in 5 tissue cultures; Kruskal–Wallis test followed by Dunn’s multiple comparisons test). **D**, Presynaptic but not postsynaptic recombination was accompanied by an increase in both uEPSC amplitude and area when compared with nonrecombined pairs of neurons (Kruskal–Wallis test followed by Dunn’s multiple comparisons test). **E**, Assessment of short-term plasticity confirmed the increase in uEPSC amplitude on presynaptic but not postsynaptic recombination. Moreover, normalized analysis revealed a more prominent synaptic depletion after both presynaptic and postsynaptic recombination (RM 2-way ANOVA with Sidak’s multiple comparisons test; statistical analysis provided in Extended Data Table 6-1, Table 6-2). Individual data points are indicated by gray dots. Values represent mean  $\pm$  SEM (\* $p < 0.05$ , \*\* $p < 0.01$ , \*\*\* $p < 0.001$ ; ns, not significant).

$U = 386$ ]. These findings are in line with our transcriptome analysis (compare Fig. 4), which indicated a differential expression of synaptic-vesicle-related genes. Therefore, we conclude that APP deficiency is accompanied by increased numbers and fractions of ready-to-release vesicles at perforant path synapses onto dentate GCs.

### Presynaptic but not postsynaptic APP restrains excitatory neurotransmission at medial perforant path synapses

Finally, we explored the impact of presynaptic and postsynaptic APP expression on excitatory synaptic transmission at medial perforant synapses. For these experiments, we used tissue cultures from *APP<sup>flox/flox</sup> × Ai14 Cre* reporter mice. Floxed APP gene recombination and Cre-dependent tdTomato expression were achieved through the local viral injection of AAV-hSyn-Cre-GFP. Postsynaptic APP deletion was achieved by viral infections in the dentate gyrus (Fig. 6A, left), and presynaptic APP deletion by Cre-GFP expression in the medial part of the entorhinal cortex in a distinct set of tissue cultures (Fig. 6A, right). Again, individual connected pairs of medial layer 2 stellate cells and dentate GCs were patched, and cellular recombination was confirmed by the somatic tdTomato fluorescence signal during the recordings (Fig. 6A,B). Presynaptic APP deficiency was accompanied by a significant reduction in synaptic failure rates (Fig. 6C; Kruskal–Wallis test with Dunn’s *post hoc* correction; no recombination–postsynaptic recombination,  $p = 0.07$ ; no recombination–presynaptic recombination,  $p = 0.002$ ). Robust increases in both the amplitude and area of successfully evoked

uEPSCs were observed (Fig. 6D; Kruskal–Wallis test with Dunn’s *post hoc* correction; uEPSC amplitude, no recombination–postsynaptic recombination,  $p = 0.28$ ; no recombination–presynaptic recombination,  $p = 0.003$ ; uEPSC area, no recombination–postsynaptic recombination,  $p = 0.22$ ; no recombination–presynaptic recombination,  $p = 0.01$ ). Conversely, postsynaptic recombination did not significantly affect synaptic transmission, although a trend toward a decrease in uEPSC failure rate should be mentioned ( $p = 0.07$ ; Fig. 6C,D). Notably, STP experiments demonstrated that both presynaptic and postsynaptic recombination were associated with synaptic depression and increased synaptic depletion compared with wild-type tissue cultures. However, only presynaptic APP deficiency resulted in higher uEPSC amplitudes (Fig. 6E; RM two-way ANOVA with Sidak’s multiple comparisons; detailed statistics provided in Extended Data Table 6-1, Table 6-2). Therefore, we conclude that excitatory neurotransmission at medial perforant path synapses is effectively restrained by presynaptic but not postsynaptic APP.

### Discussion

The role of the perforant path in normal brain function and pathologic processes has been extensively studied (Hyman et al., 1986; Witter, 2007; Robinson et al., 2014; Hainmueller and Bartos, 2018). Nevertheless, a characterization at the level of individual connected cells, that is, layer 2 stellate cells and dentate granule cells, remained challenging because of the complex three-dimensional organization of this pathway. Organotypic

entorhino-hippocampal tissue cultures provide the opportunity to investigate corticohippocampal projections in a laminated and steady-state environment characterized by *in vivo*-like ultrastructural features of excitatory synapses (Vlachos et al., 2013a; Maus et al., 2020; Galanis et al., 2021; Lenz et al., 2021). Our results show that unitary synaptic events at lateral and medial perforant path synapses are not distinct in their depolarizing effects on the soma of dentate GCs. However, trains of action potentials revealed lamina-specific differences in STP. Notably, the previously established short-term depression characteristics of the medial perforant path on a second presynaptic stimulus (Dahl and Sarvey, 1989) were not observed on the single-cell level (compare Petersen et al., 2013). As these features were evident at the level of individually connected neurons, we conclude that differences in STP at distinct excitatory inputs onto dentate GCs are related to lamina-specific synaptic properties rather than being a network phenomenon. Moreover, the properties of medial perforant path synapses depended on the presence of APP because its deficiency significantly enhanced excitatory synaptic transmission by decreasing synaptic failure rates and increasing the amplitudes and areas of uEPSCs. Increased numbers of docked vesicles at presynaptic active zones were consistently observed. Finally, we provide evidence that presynaptic but not postsynaptic APP deficiency significantly enhanced excitatory synaptic transmission, suggesting a compartment-specific regulatory role of APP.

APP is widely expressed in the CNS (Bergström et al., 2016; Del Turco et al., 2016). APP expression has been detected in excitatory and inhibitory neurons as well as glia (Haass et al., 1991; LeBlanc et al., 1997; Rohan de Silva et al., 1997; Hick et al., 2015; Mehr et al., 2020) where the cell-type-specific expression of distinct isoforms can be found (Rohan de Silva et al., 1997). In neurons, APP has primarily been found at synaptic sites (Shigematsu et al., 1992; De Strooper and Annaert, 2000; Hoe et al., 2009; Wang et al., 2009) and distinct functions have been attributed to dendritic and axonal APP (DeBoer et al., 2014). Beyond the association with pathologic conditions, such as Alzheimer's disease, its physiological roles in synaptic transmission have been recognized (Jedlicka et al., 2012; Müller et al., 2017; Hefter et al., 2020), including the regulation of excitatory and inhibitory synaptic properties, NMDA receptor trafficking, and STP. A notable feature of full-length APP is its proteolytic processing by secretases [e.g.,  $\beta$ -secretase (BACE-1) and ADAM metallopeptidase domain 10] resulting in fragments with distinct functions in regulating neural circuits (Vassar et al., 1999; Nunan and Small, 2000; Jimenez et al., 2011). Although  $A\beta$  fragments have primarily been associated with pathologic conditions (Opazo et al., 2018), neuroprotective and synaptic-plasticity-enhancing properties have been attributed to soluble APPs $\alpha$  (Jimenez et al., 2011; Fol et al., 2016; Mockett et al., 2017; Richter et al., 2018; Tan et al., 2018; Bold et al., 2022; Baltissen et al., 2023). Moreover, recent advances demonstrated that APP and specifically  $A\beta$  are regulators of homeostatic synaptic plasticity, which keep neuronal activity in a dynamic range through synaptic adaptations (Galanis et al., 2021). As APP has an impact on the homeostatic regulation of synaptic features, APP deficiency might lead to maladaptive plasticity and excitatory synaptic enhancement at medial perforant path synapses (Maggio and Vlachos, 2014). Indeed, APP deficiency was previously associated with deficits in long-term potentiation in old mice (Dawson et al., 1999; Ring et al., 2007), alterations in the network activity (Zhang et al., 2016), and a higher seizure susceptibility (Steinbach et al., 1998).

However, APP-deficient mice are viable and fertile and do not show behavioral deficits (Müller et al., 2017), which might result from compensation by APP homologs (Herms et al., 2004; Hick et al., 2015; Mehr et al., 2020; Steubler et al., 2021).

Previous studies have shown that APP can be found at the presynaptic active zone and has been suggested to have dedicated roles in the synaptic vesicle cycle (Wang et al., 2005; Yang et al., 2005; Laßek et al., 2013, 2016). Moreover, APP and its cleavage products can affect hippocampal networks (Harris et al., 2010). The release of  $A\beta$  from perforant path terminals has been found to affect synaptic integrity (Lazarov et al., 2002), which can depress excitatory synapses (Kamenetz et al., 2003; He et al., 2019). In this context, presynaptic calcium channels and vesicle recycling represent targets for  $A\beta$ , which mediates the suppression of spontaneous synaptic activity (Kelly et al., 2005; Kelly and Ferreira, 2007; Nimmrich et al., 2008). In line with these findings, we here provide evidence that presynaptic APP, which might promote localized actions of  $A\beta$  at presynaptic sites (cf. Lazarevic et al., 2017; Anni et al., 2021), is essential for restraining excitatory synaptic transmission at medial perforant path synapses on dentate GCs. These findings support recent evidence on the role of presynapses in Alzheimer's disease pathogenesis (Barthet and Mulle, 2020; Jordà-Siquier et al., 2022). In support of the restraining effects of APP and its proteolytic cleavage products, we showed that at the level of connected pairs of neurons, presynaptic APP controls the efficacy and strength of perforant path synapses. Indeed, our ultrastructure and transcriptome analyses, supported by functional data, demonstrated increased numbers of docked vesicles in the active zone of synapses and differential expression of synaptic-vesicle-related genes. This aligns with an elevated probability of vesicle release. However, no changes in STP were observed in the absence of APP. This leads to an intriguing theory that APP deficiency may interfere with vesicle docking at active zones, leaving vesicle recruitment unaltered. Notably, our study identified a correlation between the differential expression of presynaptic genes (e.g., *Nlgn1*, *Nrxn1*, *Pclo*, *Stx1b/2*, *Syn1/2* and *Syt4/10*) and the morphologic and functional states of synapses, highlighting the importance of differential gene expression patterns. Further investigation is needed to understand the molecular signals by which APP and its proteolytic cleavage product mediate these effects. However, based on our findings, we can conclude that the expression pattern of presynaptic genes facilitates a reorganization of synaptic sites, influencing both morphology and function. We are confident that our dataset makes a significant contribution toward identifying relevant transcripts involved in the APP-dependent regulation of presynaptic vesicles in future studies. In contrast, other studies have shown decreases in presynaptic vesicle abundance at neuromuscular synapses in genetic models targeting several APP-related genes (e.g., amyloid  $\beta$  precursor-like protein 2 and APP double mutants; Wang et al., 2005; Yang et al., 2005) indicating the complex regulation of presynaptic function by members of the APP protein family. Whether APP functions as an uncleaved transmembrane protein or via amyloidogenic or anti-amyloidogenic processing products at presynaptic sites warrants further investigation.

Our results demonstrate that presynaptic APP expression restrains excitatory neurotransmission at EC-GC synapses. Presynaptic APP levels are regulated through anterograde axonal transport. Several studies have shown that anterograde axonal transport is affected early in neurodegenerative diseases, which can promote amyloidogenesis (Tang, 2009; Bera et al., 2020;

Chaves et al., 2021). Moreover, APP levels in the presynaptic compartment decrease on axonal transport disturbances during neurodegeneration (Mórotz et al., 2019). Our results suggest that reduced APP levels in the presynaptic terminals of the perforant path might cause a synaptic imbalance and maladaptation through excitatory synaptic enhancement. Although neural network hyperexcitability is often observed in animal models and human subjects with Alzheimer's disease (Ghatak et al., 2019; Zott et al., 2019; Voskobiynek et al., 2020), it should be noted that neither compartment-specific nor complete APP deletion can account for the complex pathophysiology of Alzheimer's disease. However, it is interesting to speculate that defects in axonal APP transport leading to decreased presynaptic APP levels might contribute to alterations in hippocampal information processing (Haytural et al., 2020).

Information processing in the dentate gyrus is a crucial step during memory acquisition. In this regard, the pattern-separation properties of dentate GCs have been associated with performances in cognitive tasks (Leutgeb et al., 2007; Bekinschtein et al., 2013; Frank et al., 2020). The roles of STP and synaptic strength at perforant path synapses in dentate gyrus computations remain poorly understood. Our results demonstrate that compartmentalized APP deficiency significantly enhanced excitatory neurotransmission at medial perforant path synapses onto dentate GCs. We hypothesize that these alterations in excitatory perforant path neurotransmission might significantly interfere with the pattern separation abilities of the dentate gyrus network. It is interesting to theorize that behavioral deficits in Alzheimer's disease might result from presynaptically driven altered information processing in the dentate gyrus (Barthet and Mulle, 2020). Therefore, we conclude that APP deficiency at presynaptic terminals, which might be caused by genetic alterations or defects in axonal transport, could affect hippocampal information processing and memory formation.

## References

- Afgan E, Baker D, van den Beek M, Blankenberg D, Bouvier D, Čech M, Chilton J, Clements D, Coraor N, Eberhard C, Grüning B, Guerler A, Hillman-Jackson J, Von Kuster G, Rasche E, Soranzo N, Turaga N, Taylor J, Nekrutenko A, Goecks J (2016) The Galaxy platform for accessible, reproducible and collaborative biomedical analyses: 2016 update. *Nucleic Acids Res* 44(W1):W3–W10.
- Afgan E, Baker D, Batut B, van den Beek M, Bouvier D, Cech M, Chilton J, Clements D, Coraor N, Grüning BA, Guerler A, Hillman-Jackson J, Hiltemann S, Jalili V, Rasche H, Soranzo N, Goecks J, Taylor J, Nekrutenko A, Blankenberg D (2018) The Galaxy platform for accessible, reproducible and collaborative biomedical analyses: 2018 update. *Nucleic Acids Res* 46(W1):W537–W544.
- Amaral DG, Scharfman HE, Lavenex P (2007) The dentate gyrus: fundamental neuroanatomical organization (dentate gyrus for dummies). *Prog Brain Res* 163:3–22.
- Anni D, Weiss EM, Guhathakurta D, Akdas YE, Klueva J, Zeitler S, Andres-Alonso M, Huth T, Fejtova A (2021) A $\beta$ 1-16 controls synaptic vesicle pools at excitatory synapses via cholinergic modulation of synapsin phosphorylation. *Cell Mol Life Sci* 78:4973–4992.
- Baltissen D, Bold CS, Rehra L, Banićević M, Fricke J, Just J, Ludewig S, Buchholz CJ, Korte M, Müller UC (2023) APPs $\alpha$  rescues CDK5 and GSK3b dysregulation and restores normal spine density in Tau transgenic mice. *Front Cell Neurosci* 17:1106176.
- Barthet G, Mulle C (2020) Presynaptic failure in Alzheimer's disease. *Prog Neurobiol* 194:101801.
- Batut B, van den Beek M, Doyle MA, Soranzo N (2021) RNA-seq data analysis in Galaxy. *Methods Mol Biol* 2284:367–392.
- Becker D, Willems LM, Vnencak M, Zahn N, Schuldt G, Jedlicka P, Maggion D, Deller T, Vlachos A (2012) Functional and structural properties of dentate granule cells with hilar basal dendrites in mouse entorhino-hippocampal slice cultures. *PLoS One* 7:e48500.
- Beining M, Mongiat LA, Schwarzacher SW, Cuntz H, Jedlicka P (2017) T2N as a new tool for robust electrophysiological modeling demonstrated for mature and adult-born dentate granule cells. *Elife* 6:e26517.
- Bekinschtein P, Kent BA, Oomen CA, Clemenson GD, Gage FH, Saksida LM, Bussey TJ (2013) BDNF in the dentate gyrus is required for consolidation of “pattern-separated” memories. *Cell Rep* 5:759–768.
- Bera S, Cambor-Perujo S, Calleja Barca E, Negrete-Hurtado A, Racho J, De Bruyckere E, Wittich C, Ellrich N, Martins S, Adjaye J, Kononenko NL (2020) AP-2 reduces amyloidogenesis by promoting BACE1 trafficking and degradation in neurons. *EMBO Rep* 21:e47954.
- Bergström P, Agholme L, Nazir FH, Satir TM, Toombs J, Wellington H, Strandberg J, Bontell TO, Kvartsberg H, Holmström M, Boreström C, Simonsson S, Kunath T, Lindahl A, Blennow K, Hanse E, Portelius E, Wray S, Zetterberg H (2016) Amyloid precursor protein expression and processing are differentially regulated during cortical neuron differentiation. *Sci Rep* 6:29200.
- Bold CS, Baltissen D, Ludewig S, Back MK, Just J, Kilian L, Erdinger S, Banicevic M, Rehra L, Almouhanna F, Nigri M, Wolfer DP, Spilger R, Rohr K, Kann O, Buchholz CJ, von Engelhardt J, Korte M, Müller UC (2022) APPs $\alpha$  rescues tau-induced synaptic pathology. *J Neurosci* 42:5782–5802.
- Chaves RS, Tran M, Holder AR, Balcer AM, Dickey AM, Roberts EA, Bober BG, Gutierrez E, Head BP, Groisman A, Goldstein LSB, Almenar-Queral A, Shah SB (2021) Amyloidogenic processing of amyloid precursor protein drives stretch-induced disruption of axonal transport in hiPSC-derived neurons. *J Neurosci* 41:10034–10053.
- Dahl D, Sarvey JM (1989) Norepinephrine induces pathway-specific long-lasting potentiation and depression in the hippocampal dentate gyrus. *Proc Natl Acad Sci U S A* 86:4776–4780.
- Dawson GR, Seabrook GR, Zheng H, Smith DW, Graham S, O'Dowd G, Bowery BJ, Boyce S, Trumbauer ME, Chen HY, Van der Ploeg LH, Sirinathsinghji DJ (1999) Age-related cognitive deficits, impaired long-term potentiation and reduction in synaptic marker density in mice lacking the beta-amyloid precursor protein. *Neuroscience* 90:1–13.
- DeBoer SR, Dolios G, Wang R, Sisodia SS (2014) Differential release of  $\beta$ -amyloid from dendrite- versus axon-targeted APP. *J Neurosci* 34:12313–12327.
- Del Turco D, Deller T (2007) Organotypic entorhino-hippocampal slice cultures—a tool to study the molecular and cellular regulation of axonal regeneration and collateral sprouting *in vitro*. *Methods Mol Biol* 399:55–66.
- Del Turco D, Paul MH, Schlaudraff J, Hick M, Endres K, Müller UC, Deller T (2016) Region-specific differences in amyloid precursor protein expression in the mouse hippocampus. *Front Mol Neurosci* 9:134.
- De Strooper B, Annaert W (2000) Proteolytic processing and cell biological functions of the amyloid precursor protein. *J Cell Sci* 113(Pt 11):1857–1870.
- Fol R, Braudeau J, Ludewig S, Abel T, Weyer SW, Roederer JP, Brod F, Audrain M, Bemelmans AP, Buchholz CJ, Korte M, Cartier N, Müller UC (2016) Viral gene transfer of APPs $\alpha$  rescues synaptic failure in an Alzheimer's disease mouse model. *Acta Neuropathol* 131:247–266.
- Forster E, Zhao S, Frotscher M (2006) Laminating the hippocampus. *Nat Rev Neurosci* 7:259–267.
- Frank D, Montemurro MA, Montaldi D (2020) Pattern separation underpins expectation-modulated memory. *J Neurosci* 40:3455–3464.
- Frotscher M, Heimrich B (1995) Lamina-specific synaptic connections of hippocampal neurons *in vitro*. *J Neurobiol* 26:350–359.
- Galanis C, Fellenz M, Becker D, Bold C, Lichtenthaler SF, Müller UC, Deller T, Vlachos A (2021) Amyloid-beta mediates homeostatic synaptic plasticity. *J Neurosci*
- Galaxy Community (2022) The Galaxy platform for accessible, reproducible and collaborative biomedical analyses: 2022 update. *Nucleic Acids Res* 50(W1):W345–W351.
- Ghatak S, Dolatabadi N, Trudler D, Zhang X, Wu Y, Mohata M, Ambasadhan R, Talantova M, Lipton SA (2019) Mechanisms of hyperexcitability in Alzheimer's disease hiPSC-derived neurons and cerebral organoids vs isogenic controls. *Elife* 8:e50333.
- GoodSmith D, Chen X, Wang C, Kim SH, Song H, Burgalossi A, Christian KM, Knierim JJ (2017) Spatial representations of granule cells and mossy cells of the dentate gyrus. *Neuron* 93:677–690.e5.

- Haass C, Hung AY, Selkoe DJ (1991) Processing of beta-amyloid precursor protein in microglia and astrocytes favors an internal localization over constitutive secretion. *J Neurosci* 11:3783–3793.
- Hailer NP, Jarhult JD, Nitsch R (1996) Resting microglial cells in vitro: analysis of morphology and adhesion molecule expression in organotypic hippocampal slice cultures. *Glia* 18:319–331.
- Hainmueller T, Bartos M (2018) Parallel emergence of stable and dynamic memory engrams in the hippocampus. *Nature* 558:292–296.
- Harris JA, Devidze N, Verret L, Ho K, Halabisky B, Thwin MT, Kim D, Hamto P, Lo I, Yu GQ, Palop JJ, Masliah E, Mucke L (2010) Transsynaptic progression of amyloid- $\beta$ -induced neuronal dysfunction within the entorhinal-hippocampal network. *Neuron* 68:428–441.
- Hashimoto Y, Nasrallah K, Jensen KR, Chávez AE, Carrera D, Castillo PE (2017) LTP at hilar mossy cell-dentate granule cell synapses modulates dentate gyrus output by increasing excitation/inhibition balance. *Neuron* 95:928–943.e3.
- Haytural H, Mermelekas G, Emre C, Nigam SM, Carroll SL, Winblad B, Bogdanovic N, Barthelet G, Granholm AC, Orre LM, Tjernberg LO, Frykman S (2020) The proteome of the dentate terminal zone of the perforant path indicates presynaptic impairment in Alzheimer disease. *Mol Cell Proteomics* 19:128–141.
- He Y, Wei M, Wu Y, Qin H, Li W, Ma X, Cheng J, Ren J, Shen Y, Chen Z, Sun B, Huang FD, Shen Y, Zhou YD (2019) Amyloid  $\beta$  oligomers suppress excitatory transmitter release via presynaptic depletion of phosphatidylinositol-4,5-bisphosphate. *Nat Commun* 10:1193.
- Heber S, Herms J, Gajic V, Hainfellner J, Aguzzi A, Rülcke T, von Kretschmar H, von Koch C, Sisodia S, Tremml P, Lipp HP, Wolf DP, Müller U (2000) Mice with combined gene knock-outs reveal essential and partially redundant functions of amyloid precursor protein family members. *J Neurosci* 20:7951–7963.
- Hefter D, Ludewig S, Draguhn A, Korte M (2020) Amyloid, APP, and electrical activity of the brain. *Neuroscientist* 26:231–251.
- Henze DA, Buzsaki G (2007) Hilar mossy cells: functional identification and activity *in vivo*. *Prog Brain Res* 163:199–216.
- Herms J, Anliker B, Heber S, Ring S, Fuhrmann M, Kretschmar H, Sisodia S, Müller U (2004) Cortical dysplasia resembling human type 2 lissencephaly in mice lacking all three APP family members. *EMBO J* 23:4106–4115.
- Hick M, Herrmann U, Weyer SW, Mallm JP, Tschape JA, Borgers M, Mercken M, Roth FC, Draguhn A, Slomianka L, Wolf DP, Korte M, Müller UC (2015) Acute function of secreted amyloid precursor protein fragment APPs $\beta$  in synaptic plasticity. *Acta Neuropathol* 129:21–37.
- Hines ML, Carnevale NT (1997) The NEURON simulation environment. *Neural Comput* 9:1179–1209.
- Hoe HS, Fu Z, Makarova A, Lee JY, Lu C, Feng L, Pajoohesh-Ganji A, Matsuoka Y, Hyman BT, Ehlers MD, Vicini S, Pak DT, Rebeck GW (2009) The effects of amyloid precursor protein on postsynaptic composition and activity. *J Biol Chem* 284:8495–8506.
- Hsu D (2007) The dentate gyrus as a filter or gate: a look back and a look ahead. *Prog Brain Res* 163:601–613.
- Humpel C (2015) Organotypic brain slice cultures: a review. *Neuroscience* 305:86–98.
- Hyman BT, Van Hoesen GW, Kromer LJ, Damasio AR (1986) Perforant pathway changes and the memory impairment of Alzheimer's disease. *Ann Neurol* 20:472–481.
- Jalili V, Afgan E, Gu Q, Clements D, Blankenberg D, Goecks J, Taylor J, Nekrutenko A (2020) The Galaxy platform for accessible, reproducible and collaborative biomedical analyses: 2020 update. *Nucleic Acids Res* 48(W1):W395–W402.
- Jedlicka P, Owen M, Vnencak M, Tschäpe JA, Hick M, Müller UC, Deller T (2012) Functional consequences of the lack of amyloid precursor protein in the mouse dentate gyrus *in vivo*. *Exp Brain Res* 217:441–447.
- Jiang R, Wu XF, Wang B, Guan RX, Lv LM, Li AP, Lei L, Ma Y, Li N, Li QF, Ma QH, Zhao J, Li S (2020) Reduction of Ngr in perforant path decreases amyloid-beta peptide production and ameliorates synaptic and cognitive deficits in APP/PS1 mice. *Alzheimers Res Ther* 12:47.
- Jimenez S, Torres M, Vizuet M, Sanchez-Varo R, Sanchez-Mejias E, Trujillo-Estrada L, Carmona-Cuenca I, Caballero C, Ruano D, Gutierrez A, Vitorica J (2011) Age-dependent accumulation of soluble amyloid beta (A $\beta$ ) oligomers reverses the neuroprotective effect of soluble amyloid precursor protein-alpha (sAPP(alpha)) by modulating phosphatidylinositol 3-kinase (PI3K)/Akt-GSK-3beta pathway in Alzheimer mouse model. *J Biol Chem* 286:18414–18425.
- Jonas P, Lisman J (2014) Structure, function, and plasticity of hippocampal dentate gyrus microcircuits. *Front Neural Circuits* 8:107.
- Jordà-Siquier T, Petrel M, Kouskoff V, Smailovic U, Cordelières F, Frykman S, Müller U, Mülle C, Barthelet G (2022) APP accumulates with presynaptic proteins around amyloid plaques: a role for presynaptic mechanisms in Alzheimer's disease? *Alzheimers Dement* 18:2099–2116.
- Kamenetz F, Tomita T, Hsieh H, Seabrook G, Borchelt D, Iwatsubo T, Sisodia S, Malinow R (2003) APP processing and synaptic function. *Neuron* 37:925–937.
- Kelly BL, Ferreira A (2007) Beta-amyloid disrupted synaptic vesicle endocytosis in cultured hippocampal neurons. *Neuroscience* 147:60–70.
- Kelly BL, Vassar R, Ferreira A (2005) Beta-amyloid-induced dynamin 1 depletion in hippocampal neurons. A potential mechanism for early cognitive decline in Alzheimer disease. *J Biol Chem* 280:31746–31753.
- Kirkby DL, Higgins GA (1998) Characterization of perforant path lesions in rodent models of memory and attention. *Eur J Neurosci* 10:823–838.
- Krook-Magnuson E, Armstrong C, Bui A, Lew S, Oijala M, Soltesz I (2015) *In vivo* evaluation of the dentate gate theory in epilepsy. *J Physiol* 593:2379–2388.
- Krueppel R, Remy S, Beck H (2011) Dendritic integration in hippocampal dentate granule cells. *Neuron* 71:512–528.
- Lašek M, Weingarten J, Einsfelder U, Brendel P, Müller U, Volkandt W (2013) Amyloid precursor proteins are constituents of the presynaptic active zone. *J Neurochem* 127:48–56.
- Lašek M, Weingarten J, Wegner M, Mueller BF, Rohmer M, Baeumlisberger D, Arrey TN, Hick M, Ackermann J, Acker-Palmer A, Koch I, Müller U, Karas M, Volkandt W (2016) APP is a context-sensitive regulator of the hippocampal presynaptic active zone. *PLoS Comput Biol* 12:e1004832.
- Lazarevic V, Fienko S, Andres-Alonso M, Anni D, Ivanova D, Montenegro-Venegas C, Gundelfinger ED, Cousin MA, Fejtova A (2017) Physiological concentrations of amyloid beta regulate recycling of synaptic vesicles via alpha7 acetylcholine receptor and CDK5/calcineurin signaling. *Front Mol Neurosci* 10:221.
- Lazarov O, Lee M, Peterson DA, Sisodia SS (2002) Evidence that synaptically released beta-amyloid accumulates as extracellular deposits in the hippocampus of transgenic mice. *J Neurosci* 22:9785–9793.
- LeBlanc AC, Papadopoulos M, Bélair C, Chu W, Crosato M, Powell J, Goodyer CG (1997) Processing of amyloid precursor protein in human primary neuron and astrocyte cultures. *J Neurochem* 68:1183–1190.
- Lenz M, Galanis C, Kleidonas D, Fellenz M, Deller T, Vlachos A (2019) Denervated mouse dentate granule cells adjust their excitatory but not inhibitory synapses following *in vitro* entorhinal cortex lesion. *Exp Neurol* 312:1–9.
- Lenz M, Eichler A, Kruse P, Muellerleile J, Deller T, Jedlicka P, Vlachos A (2021) All-trans retinoic acid induces synaptopodin-dependent metaplasticity in mouse dentate granule cells. *Elife* 10:e71983.
- Leutgeb JK, Moser EI (2007) Enigmas of the dentate gyrus. *Neuron* 55:176–178.
- Leutgeb JK, Leutgeb S, Moser MB, Moser EI (2007) Pattern separation in the dentate gyrus and CA3 of the hippocampus. *Science* 315:961–966.
- Li ZW, Stark G, Götz J, Rülcke T, Gschwind M, Huber G, Müller U, Weissmann C (1996) Generation of mice with a 200-kb amyloid precursor protein gene deletion by Cre recombinase-mediated site-specific recombination in embryonic stem cells. *Proc Natl Acad Sci U S A* 93:6158–6162.
- Love MI, Huber W, Anders S (2014) Moderated estimation of fold change and dispersion for RNA-seq data with DESeq2. *Genome Biol* 15:550.
- Madisen L, Zwingman TA, Sunkin SM, Oh SW, Zariwala HA, Gu H, Ng LL, Palminter RD, Hawrylycz MJ, Jones AR, Lein ES, Zeng H (2010) A robust and high-throughput Cre reporting and characterization system for the whole mouse brain. *Nat Neurosci* 13:133–140.
- Maggio N, Vlachos A (2014) Synaptic plasticity at the interface of health and disease: new insights on the role of endoplasmic reticulum intracellular calcium stores. *Neuroscience* 281:135–146.
- Mallm JP, Tschäpe JA, Hick M, Filippov MA, Müller UC (2010) Generation of conditional null alleles for APP and APLP2. *Genesis* 48:200–206.
- Maus L, Lee C, Altas B, Sertel SM, Weyand K, Rizzoli SO, Rhee J, Brose N, Imig C, Cooper BH (2020) Ultrastructural correlates of presynaptic functional heterogeneity in hippocampal synapses. *Cell Rep* 30:3632–3643.e8.
- Mehr A, Hick M, Ludewig S, Muller M, Herrmann U, von Engelhardt J, Wolf DP, Korte M, Müller UC (2020) Lack of APP and APLP2 in GABAergic forebrain neurons impairs synaptic plasticity and cognition. *Cereb Cortex* 30:4044–4063.

- Mockett BG, Richter M, Abraham WC, Muller UC (2017) Therapeutic potential of secreted amyloid precursor protein APPs $\alpha$ . *Front Mol Neurosci* 10:30.
- Mórotz GM, Glennon EB, Greig J, Lau DHW, Bhembre N, Mattedi F, Muschalik N, Noble W, Vagnoni A, Miller CCJ (2019) Kinesin light chain-1 serine-460 phosphorylation is altered in Alzheimer's disease and regulates axonal transport and processing of the amyloid precursor protein. *Acta Neuropathol Commun* 7:200.
- Müller UC, Deller T, Korte M (2017) Not just amyloid: physiological functions of the amyloid precursor protein family. *Nat Rev Neurosci* 18:281–298.
- Nimmrich V, Grimm C, Draguhn A, Barghorn S, Lehmann A, Schoemaker H, Hillen H, Gross G, Ebert U, Bruehl C (2008) Amyloid beta oligomers (A $\beta$ 1–42) globulomer suppress spontaneous synaptic activity by inhibition of P/Q-type calcium currents. *J Neurosci* 28:788–797.
- Nunan J, Small DH (2000) Regulation of APP cleavage by alpha-, beta- and gamma-secretases. *FEBS Lett* 483:6–10.
- Opazo P, Viana da Silva S, Carta M, Breillat C, Coultrap SJ, Grillo-Bosch D, Sainlos M, Coussen F, Bayer KU, Mülle C, Choquet D (2018) CaMKII metaplasticity drives A $\beta$  oligomer-mediated synaptotoxicity. *Cell Rep* 23:3137–3145.
- Patton PE, McNaughton B (1995) Connection matrix of the hippocampal formation: I. The dentate gyrus. *Hippocampus* 5:245–286.
- Petersen RP, Moradpour F, Eadie BD, Shin JD, Kannangara TS, Delaney KR, Christie BR (2013) Electrophysiological identification of medial and lateral perforant path inputs to the dentate gyrus. *Neuroscience* 252:154–168.
- Ribak CE, Shapiro LA (2007) Ultrastructure and synaptic connectivity of cell types in the adult rat dentate gyrus. *Prog Brain Res* 163:155–166.
- Richter MC, Ludewig S, Winschel A, Abel T, Bold C, Salzburger LR, Klein S, Han K, Weyer SW, Fritz AK, Laube B, Wolfer DP, Buchholz CJ, Korte M, Müller UC (2018) Distinct *in vivo* roles of secreted APP ectodomain variants APPs $\alpha$  and APPs $\beta$  in regulation of spine density, synaptic plasticity, and cognition. *EMBO J* 37:
- Ring S, Weyer SW, Kilian SB, Waldron E, Pietrzik CU, Filippov MA, Herms J, Buchholz C, Eckman CB, Korte M, Wolfer DP, Müller UC (2007) The secreted beta-amyloid precursor protein ectodomain APPs alpha is sufficient to rescue the anatomical, behavioral, and electrophysiological abnormalities of APP-deficient mice. *J Neurosci* 27:7817–7826.
- Robinson JL, Molina-Porcel L, Corrada MM, Raible K, Lee EB, Lee VM, Kawas CH, Trojanowski JQ (2014) Perforant path synaptic loss correlates with cognitive impairment and Alzheimer's disease in the oldest-old. *Brain* 137:2578–2587.
- Rohan de Silva HA, Jen A, Wickenden C, Jen LS, Wilkinson SL, Patel AJ (1997) Cell-specific expression of beta-amyloid precursor protein isoform mRNAs and proteins in neurons and astrocytes. *Brain Res Mol Brain Res* 47:147–156.
- Roy DS, Arons A, Mitchell TI, Pignatelli M, Ryan TJ, Tonegawa S (2016) Memory retrieval by activating engram cells in mouse models of early Alzheimer's disease. *Nature* 531:508–512.
- Scharfman HE (1995) Electrophysiological evidence that dentate hilar mossy cells are excitatory and innervate both granule cells and interneurons. *J Neurophysiol* 74:179–194.
- Scharfman HE, Schwartzkroin PA (1988) Electrophysiology of morphologically identified mossy cells of the dentate hilus recorded in guinea pig hippocampal slices. *J Neurosci* 8:3812–3821.
- Schmidt-Hieber C, Jonas P, Bischofberger J (2007) Subthreshold dendritic signal processing and coincidence detection in dentate gyrus granule cells. *J Neurosci* 27:8430–8441.
- Scimemi A, Schorge S, Kullmann DM, Walker MC (2006) Epileptogenesis is associated with enhanced glutamatergic transmission in the perforant path. *J Neurophysiol* 95:1213–1220.
- Senzai Y, Buzsáki G (2017) Physiological properties and behavioral correlates of hippocampal granule cells and mossy cells. *Neuron* 93:691–704.e5.
- Shigematsu K, McGeer PL, McGeer EG (1992) Localization of amyloid precursor protein in selective postsynaptic densities of rat cortical neurons. *Brain Res* 592:353–357.
- Sjöström PJ, Häusser M (2006) A cooperative switch determines the sign of synaptic plasticity in distal dendrites of neocortical pyramidal neurons. *Neuron* 51:227–238.
- Smith LA, McMahon LL (2018) Deficits in synaptic function occur at medial perforant path-dentate granule cell synapses prior to Schaffer collateral-CA1 pyramidal cell synapses in the novel TgF344-Alzheimer's disease rat model. *Neurobiol Dis* 110:166–179.
- Soldano A, Hassan BA (2014) Beyond pathology: APP, brain development and Alzheimer's disease. *Curr Opin Neurobiol* 27:61–67.
- Steinbach JP, Müller U, Leist M, Li ZW, Nicotera P, Aguzzi A (1998) Hypersensitivity to seizures in beta-amyloid precursor protein deficient mice. *Cell Death Differ* 5:858–866.
- Steubler V, Erdinger S, Back MK, Ludewig S, Fässler D, Richter M, Han K, Slomianka L, Amrein I, von Engelhardt J, Wolfer DP, Korte M, Müller UC (2021) Loss of all three APP family members during development impairs synaptic function and plasticity, disrupts learning, and causes an autism-like phenotype. *EMBO J* 40:e107471.
- Subramanian A, Tamayo P, Mootha VK, Mukherjee S, Ebert BL, Gillette MA, Paulovich A, Pomeroy SL, Golub TR, Lander ES, Mesirov JP (2005) Gene set enrichment analysis: a knowledge-based approach for interpreting genome-wide expression profiles. *Proc Natl Acad Sci U S A* 102:15545–15550.
- Tamamaki N, Nojyo Y (1993) Projection of the entorhinal layer II neurons in the rat as revealed by intracellular pressure-injection of neurobiotin. *Hippocampus* 3:471–480.
- Tan VTY, Mockett BG, Ohline SM, Parfitt KD, Wicky HE, Peppercorn K, Schoderboeck L, Yahaya MFB, Tate WP, Hughes SM, Abraham WC (2018) Lentivirus-mediated expression of human secreted amyloid precursor protein-alpha prevents development of memory and plasticity deficits in a mouse model of Alzheimer's disease. *Mol Brain* 11:7.
- Tang BL (2009) Neuronal protein trafficking associated with Alzheimer disease: from APP and BACE1 to glutamate receptors. *Cell Adh Migr* 3:118–128.
- Trimper JB, Galloway CR, Jones AC, Mandi K, Manns JR (2017) Gamma oscillations in rat hippocampal subregions dentate gyrus, CA3, CA1, and subiculum underlie associative memory encoding. *Cell Rep* 21:2419–2432.
- Vassar R, et al. (1999) Beta-secretase cleavage of Alzheimer's amyloid precursor protein by the transmembrane aspartic protease BACE. *Science* 286:735–741.
- Vlachos A, Becker D, Jedlicka P, Winkels R, Roeper J, Deller T (2012a) Entorhinal denervation induces homeostatic synaptic scaling of excitatory postsynapses of dentate granule cells in mouse organotypic slice cultures. *PLoS One* 7:e32883.
- Vlachos A, Bas Orth C, Schneider G, Deller T (2012b) Time-lapse imaging of granule cells in mouse entorhino-hippocampal slice cultures reveals changes in spine stability after entorhinal denervation. *J Comp Neurol* 520:1891–1902.
- Vlachos A, Muller-Dahlhaus F, Rosskopf J, Lenz M, Ziemann U, Deller T (2012c) Repetitive magnetic stimulation induces functional and structural plasticity of excitatory postsynapses in mouse organotypic hippocampal slice cultures. *J Neurosci* 32:17514–17523.
- Vlachos A, Ikenberg B, Lenz M, Becker D, Reifenberg K, Bas-Orth C, Deller T (2013a) Synaptopodin regulates denervation-induced homeostatic synaptic plasticity. *Proc Natl Acad Sci U S A* 110:8242–8247.
- Vlachos A, Reddy-Alla S, Papadopoulos T, Deller T, Betz H (2013b) Homeostatic regulation of gephyrin scaffolds and synaptic strength at mature hippocampal GABAergic postsynapses. *Cereb Cortex* 23:2700–2711.
- Voskobiyuk Y, Roth JR, Cochran JN, Rush T, Carullo NV, Mesina JS, Waqas M, Vollmer RM, Day JJ, McMahon LL, Roberson ED (2020) Alzheimer's disease risk gene BIN1 induces Tau-dependent network hyperexcitability. *Elife* 9:e57354.
- Wang P, Yang G, Mosier DR, Chang P, Zaidi T, Gong YD, Zhao NM, Dominguez B, Lee KF, Gan WB, Zheng H (2005) Defective neuromuscular synapses in mice lacking amyloid precursor protein (APP) and APP-like protein 2. *J Neurosci* 25:1219–1225.
- Wang Z, Wang B, Yang L, Guo Q, Aithmitti N, Songyang Z, Zheng H (2009) Presynaptic and postsynaptic interaction of the amyloid

- precursor protein promotes peripheral and central synaptogenesis. *J Neurosci* 29:10788–10801.
- Winkels R, Jedlicka P, Weise FK, Schultz C, Deller T, Schwarzacher SW (2009) Reduced excitability in the dentate gyrus network of betaIV-spectrin mutant mice *in vivo*. *Hippocampus* 19:677–686.
- Winson J, Abzug C (1977) Gating of neuronal transmission in the hippocampus: efficacy of transmission varies with behavioral state. *Science* 196:1223–1225.
- Witter MP (2007) The perforant path: projections from the entorhinal cortex to the dentate gyrus. *Prog Brain Res* 163:43–61.
- Wu T, Hu E, Xu S, Chen M, Guo P, Dai Z, Feng T, Zhou L, Tang W, Zhan L, Fu X, Liu S, Bo X, Yu G (2021) clusterProfiler 4.0: A universal enrichment tool for interpreting omics data. *Innovation (Camb)* 2:100141.
- Yang G, Gong YD, Gong K, Jiang WL, Kwon E, Wang P, Zheng H, Zhang XF, Gan WB, Zhao NM (2005) Reduced synaptic vesicle density and active zone size in mice lacking amyloid precursor protein (APP) and APP-like protein 2. *Neurosci Lett* 384:66–71.
- Zhang X, Zhong W, Brankač J, Weyer SW, Müller UC, Tort AB, Draguhn A (2016) Impaired theta-gamma coupling in APP-deficient mice. *Sci Rep* 6:21948.
- Zhou B, Lu JG, Siddu A, Wernig M, Südhof TC (2022) Synaptogenic effect of APP-Swedish mutation in familial Alzheimer's disease. *Sci Transl Med* 14:eabn9380.
- Zott B, Simon MM, Hong W, Unger F, Chen-Engerer HJ, Frosch MP, Sakmann B, Walsh DM, Konnerth A (2019) A vicious cycle of  $\beta$  amyloid-dependent neuronal hyperactivation. *Science* 365:559–565.